Synthesis and Characterization of Single Crystal Kagomé Lattice Antiferromagnets

by

Tianheng Han

BSc Physics

Hong Kong University of Science and Technology (2006)

Submitted to the Department of Physics in partial fulfillment of the requirements for the degree of

Master of Science in Physics

at the

MASSACHUSETTS INSTITUTE OF TECHNOLOGY

February 2010

Author.....

Department of Physics

January 15, 2010

Certified by.....

Young S. Lee

Mark Hyman Jr. Career Development Professor, Associate Professor

Thesis Surpervisor

Accepted by.....

Krishna Rajagopal

Professor, Associate Department Head for Education

Synthesis and Characterization of Single Crystal Kagomé Lattice Antiferromagnets

by

Tianheng Han

Submitted to the Department of Physics
on January 15, 2010, in partial fulfillment of the
requirements for the degree of
Master of Science in Physics

Abstract

An ideal spin-½ kagomé lattice has been a long sought material. This system is characterized by strong magnetic frustration and is a likely candidate for a spin-liquid ground state. The spin-liquid state was originally proposed to exist in the parent compounds of the high temperature superconducting cuprates as originally proposed by Anderson. However, the lack of ideal samples have hampered experimental tests of the theories. A few years ago, a kagomé lattice material called herbertsmithite ($ZnCu_3(OH)_6Cl_2$) has been successfully synthesized and studied. Since then, many experiments have been performed which have produced a lot of new guidance for our theoretical understanding of this frustrated magnetic system. However, single crystals are crucial for further progress.

We have successfully produced high quality single crystals $ZnCu_3(OH)_6Cl_2$. These crystals are large enough for measurements, such as x-ray diffraction, magnetism, heat capacity, neutron scattering, thermal conductivity, muon-scattering and optical measurement. In this thesis, I will summarize the current state of knowledge for herbertsmithite and its family, the single crystal growth technique, and characterization of the resulting samples. A discussion of further directions of growth and measurement is at the end.

Thesis supervisor: Young S. Lee
Title: Mark Hyman Jr. Career Development Professor and Associate Professor

To my loving wife, who has always been supporting me

Acknowledgement

Without any doubt, the first person I want to say thank to is Prof. Young S. Lee, my thesis supervisor. It is him who led me into this amazing field of science. It is him whose wisdom inspires me to overcome all those tough problems. Prof. Young S. Lee's pursue of better accuracy in experiments encouraged me to advance my experimental techniques and understanding of theories. His great personality will continue to benefit me in my future study towards Ph.D.

I also want to thank my wife, Mrs.Wenjie Zhang. Whenever I lost confidence, she has always been there backing me up. She is a great woman both at work and home. Her wonderful cooking has made our life very enjoyable. Her optimism has lightened the road ahead of me.

I owe a lot of thanks to my groupmate, Dr. Joel S. Helton. Joel was a senior graduate student during my first three years at MIT. He has a deep understanding of condensed matter physics and a lot of patience in teaching me how to do experiments. He is like a big brother for me. Without him, I could not have learnt so much.

Dr. Shaoyan Chu, a research scientist from the center of material science and engineer, has given me a lot of advices on crystal growth. I have learned from every conversation with him. He is a wonderful person to work with and learn from.

I am very lucky to have a very cooperative group, Dr. Deepak Singh, Dr. Andrea Prodi, Dr. Kittiwit Matan, Craig Bonnoit, Robin Chisnell and Dillon Gardner. Working with them has been a wonderful experience. My collaboration with NIST's scientists, Prof. Jeffery Lynn, Dr. Sung Chang and Dr. Ying Chen, was a great opportunity for researching and learning. Dr. Emily Nykto, a former graduate student in Nocera's Chemistry group at MIT, has helped me a lot in the synthesis of Zn-paratacamite. Dr. Peter Mueller, a research scientist from Chemistry department at MIT, has given me a lot of help for single crystal X-ray diffraction.

At last, I appreciate my parents for giving me early education on science. They have paid special attention in building up my interest in science and have been my first teachers. Gradually, I became attracted by the mystery of the universe. I will do my best for their sake.

Contents

1. Introduction **15**

1.1 Geometric magnetic frustration.....16

1.2 Zn-paratacamite family.....23

1.3 Synthesis of powder herbertsmithite.....27

1.4 Thesis outline.....29

2. Experimental Techniques **31**

2.1 Three Zone furnace.....31

2.2 Inductive Coupled Plasma (ICP).....32

2.3 SQUID.....33

2.4 Neutron Source and Triple Axis Spectrometer.....35

3. Herbertsmithite Single Crystal Growth **39**

3.1 Motivation.....39

3.2 Crystal Growth Technique.....40

3.3 Improvement of Growth Technique.....43

3.4 Summary.....45

4. Characterization of Single Crystal Herbertsmithite **47**

4.1 Chemical Analysis.....47

4.2 Structural Determination.....50

4.3 Structural Neutron Scattering Measurement.....53

4.4 Magnetic Property.....55

4.5 Summary.....59

5. Discussion **61**

5.1 Problems on current crystal growth.....61

5.2 Coaligning Crystals.....62

5.3 Future studies of single crystal herbertsmithite.....63

5.4 Summary.....64

Appendix A. Crystallographic Data for HTH_1_11 **71**

Appendix B. Crystallographic Data for HTH_4_41 **81**

List of Figures

1-1 Neel order on 2D square lattice.....16

1-2 Magnetic frustration on 2D triangular lattice.....17

1-3 Heisenburg spin chirality on a triangle.....18

1-4 Edge shareing triangular lattice and Kagomé Lattice.....19

1-5 Spin configurations for two neighboring triangles.....19

1-6 Structural unit cells, magnetic unit cells and zero energy modes on edge shareing triangular lattice and Kagomé Lattice.....20

1-7 Structure of herbertsmithite with only Copper and Zinc.....25

1-8 ABC stacking of kagomé layers in herbertsmithite.....25

1-9 Rhombohedral unit cell structure of herbertsmithite, $ZnCu_3(OH)_6Cl_2$.....26

2-1 Schematic of inductive coupled plasma (ICP).....33

2-2 Schematic of a triple axis spectrometer.....36

3-1 Schematic for herbertsmithite single crystal growth in three zone furnace.....41

3-2 The biggest herbertsmithite ($Zn_{0.89}Cu_{3.11}(OH)_6Cl_2$) sample HTH_3_31.....43

4-1 x value Vs $100xN_{Zn}/N_{H2O}$.....49

4-2 Crystal orientation determination.....52

4-3 Crystal structure of herbertsmithite.....53

4-4 Mosaic of HTH_3_31.....55

4-5 Magnetic susceptibility of HTH-1-1 and MPS-6-135.....57

4-6 Inverse magnetic susceptibility fitting for HTH_1_1.....58

4-7 Field cool and zero field cool magnetic susceptibility of HTH_1_1.....58

5-1 Crystal coaligning.....63

List of Tables

4-1 ICP results summary.....48

4-2 Crystallographic data for herbertsmithite.....51

Chapter 1

Introduction

Perfect two-dimensional spin-1/2 kagomé antiferromagnet features strong geometric magnetic frustration[1, 2] and larger quantum spin fluctuation. Philip W Anderson has proposed that spin liquid may be an alternative ground state to Neel order[3]. Spin liquid does not have any magnetic order or symmetry breaking down to very low temperature. It is proposed to be present in high T_c-cuprates' parent compounds[4]. Herbertsmithite, a family member of Zn-paratacamite minerals, is the first realized perfect spin-1/2 kagomé antiferromagnet. All earlier compounds have either larger spins or structure distortions. For herbertsmithite, no magnetic ordering has been observed down to much lower temperature than its Curie-Wiess temperature[5]. It is an excellent candidate for spin liquid and strong frustrated antiferromagnetism[6], attracting tremendous attentions, both theoretical and experimental.

1.1 Geometric magnetic frustration

Let's consider a two-dimensional lattice. On a two dimensional square lattice as in Fig. 1-1, suppose each lattice site has a spin. If the nearest neighbor interaction is antiferromagnetic, then the spin lattice can settle down to the configuration shown, called Neel order[7]. The exchange energy between two neighboring spins is expressed as[8]

$$H = 2 J S_1 S_2 \tag{1.1}$$

with positive J. Every interaction's energy is minimized to $-2JS^2$, so there is no frustration. The only degeneracy for this system is a global rotation of all the spins.

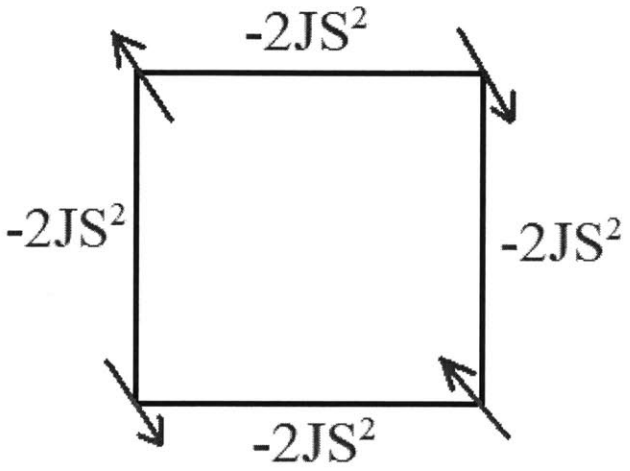

Figure 1-1: Neel order on 2D square lattice with exchange energies shown.

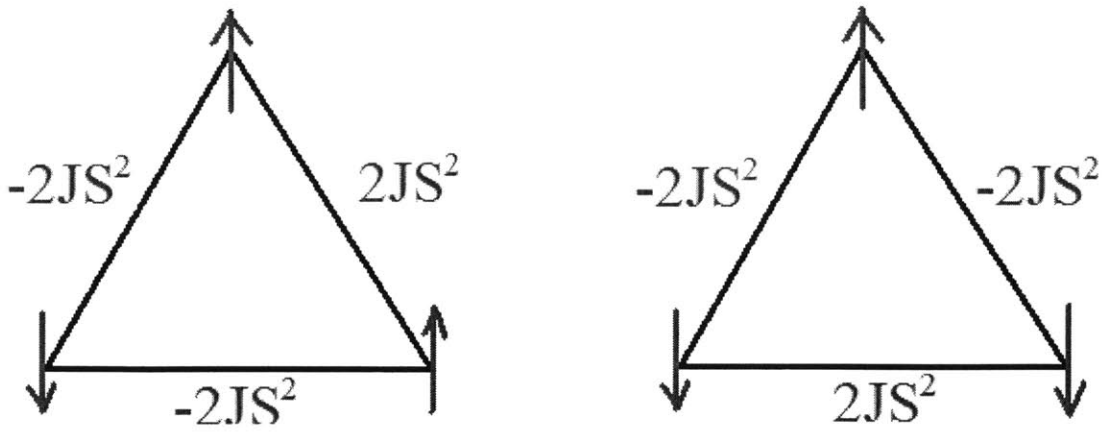

Figure 1-2: Magnetic frustration on 2D triangular lattice with exchange energies shown. Ising spin is assumed. The right bottom spin has a two-fold degeneracy with equal total energies.

In contrast to this, let's consider a two-dimensional triangular lattice with Ising spins[9] in Fig. 1-2. When two spins are antiparrallel to each other, the third spin does not know which way, up or down, to get aligned. The two configurations have equal total energies, $-2JS_2$, compared to $-6JS_2$ if all exchange energies are minimized. So, frustration increases the total energy of the system. With Ising spins, there is a two-fold degeneracy on top of a global rotation of all the spins. This frustration can be released if we consider Heisenberg spins. There are two ways for releasing the frustration. In Fig. 1-3 left, the three spins have positive chirality[10] +1 while in Fig. 1-3 right the three spins have chirality -1. Chirality is defined as

$$\vec{K} = \frac{2}{3\sqrt{3}} (\vec{S}_1 \times \vec{S}_2 + \vec{S}_2 \times \vec{S}_3 + \vec{S}_3 \times \vec{S}_1) \qquad (1.2)$$

where the S_1 S_2 S_3 are arranged counter-clockwisely. In each case, the total energy is reduced to $-3JS_2$, still higher than $-6JS_2$. Thus, the frustration is only partially released.

There is an easy way to tell the chirality of three spins on a triangle. Let's consider those three spins clockwisely, that is, $S_1 \rightarrow S_3 \rightarrow S_2 \rightarrow S_1$. For chirality +1, we rotate S_1 clockwisely (looking into the paper) by 120 degrees to get S_3. For $S_3 \rightarrow S_2$ and $S_2 \rightarrow S_1$, we also rotate the spin by 120 degrees clockwisely. For chirality -1, we rotate S_1 counter-clockwisely (looking into the paper) by 120 degrees to get S_3. For $S_3 \rightarrow S_2$ and $S_2 \rightarrow S_1$, we also rotate the spin by 120 degrees counter-clockwisely.

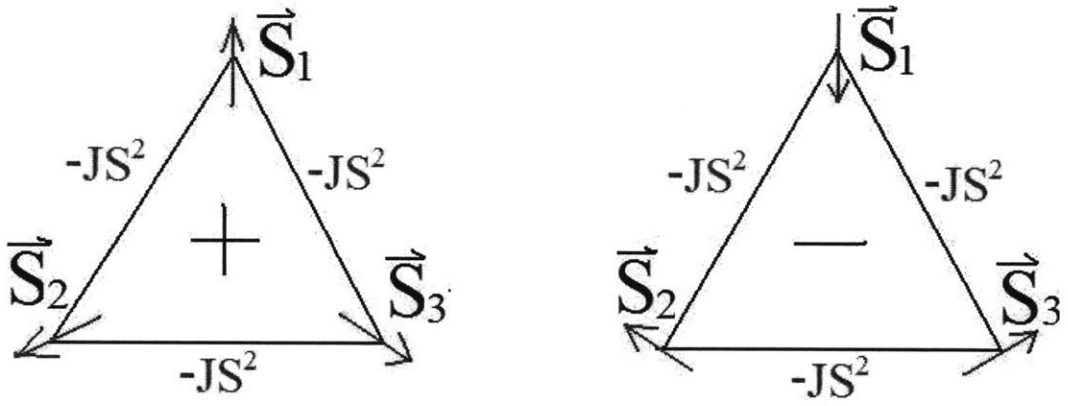

Figure 1-3: Heisenburg spin chirality on a triangle. The left one has spin chirality +1 (indicated by + inside) while the right one has spin chirality -1 (indicated by – inside). The total energies and the energies for each exchange path way are identical for both cases.

There are two different triangular lattices, edge sharing and corner sharing, as shown in Fig. 1-4. Corner sharing triangular lattice got the name Kagomé lattice due to the similarity with a kind of Japanese basket named Kagomé, where Kago means basket and mé means hole[11]. Kagomé lattice is the structure on which this thesis focuses on.

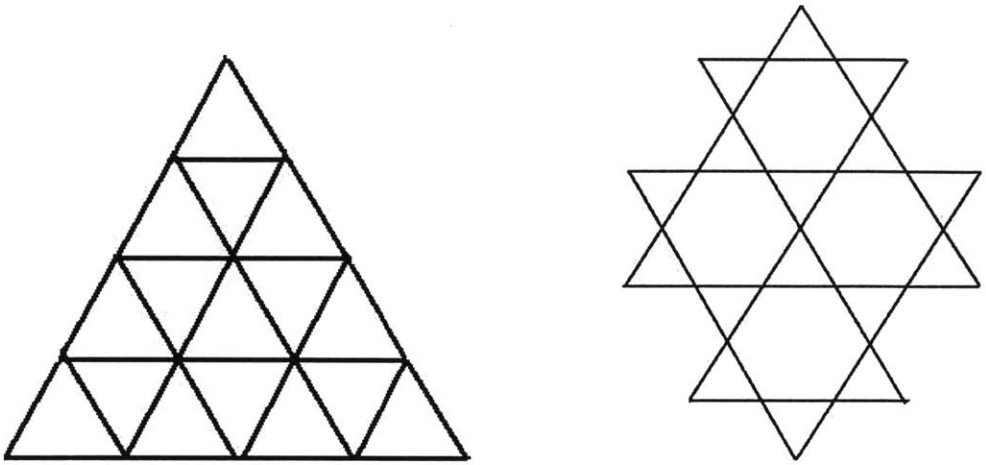

Figure 1-4: Edge shareing triangular lattice (left) and corner sharing triangular lattice called Kagomé Lattice (right).

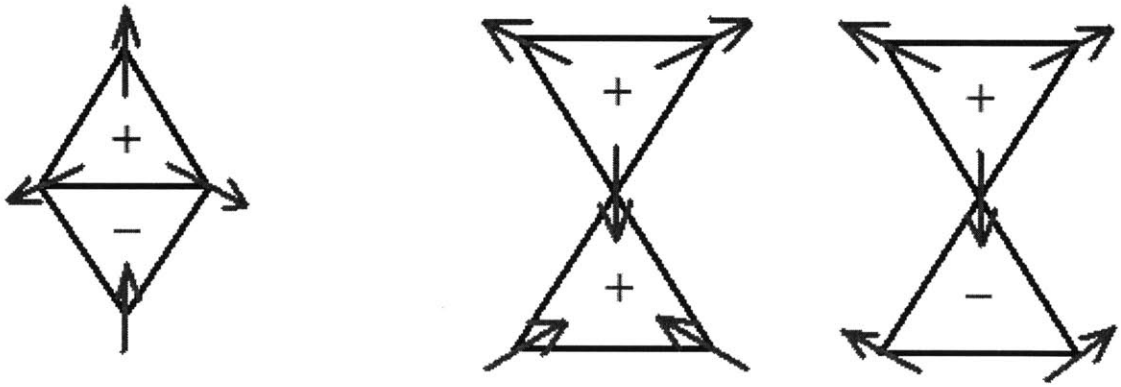

Figure 1-5: Spin configurations for two neighboring triangles. Left: edge sharing triangles. Middle and right: Kagomé corner sharing triangles. + indicates chirality +1 and – indicates chirality -1.

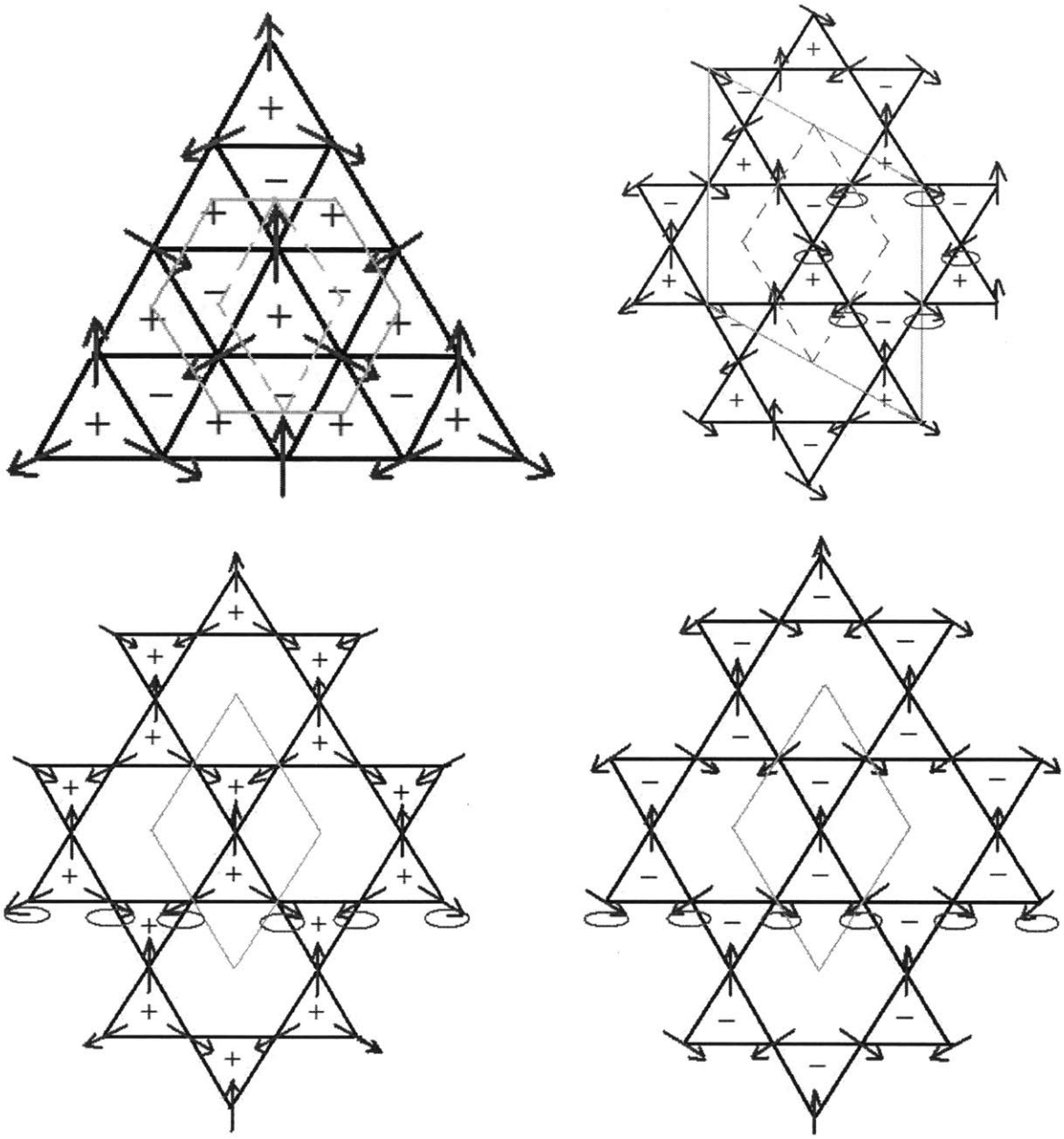

Figure 1-6: In each figure, the structure unit cell is circled by dotted orange lines and magnetic unit cell is circled by solid green lines. Structure unit cell and magnetic unit cell are identical for the bottom two figures. Upper left: edge sharing triangular lattice with staggered chirality. Upper right: $\sqrt{3}$ x $\sqrt{3}$ staggered chirality Kagomé lattice. The magnetic unit cell is three times larger than structural unit cell. Bottom left: Kagomé lattice in q=0 state with uniform chirality +1. Bottom right: Kagomé lattice in q=0 state with uniform chirality -1. The blue ellipses show simultaneous spin rotations of zero energy modes.

Although both antiferromagnetic edge sharing triangular lattice and Kagomé lattice have magnetic frustrations, the latter one has more. There are several reasons. Let's consider a local spin arrangement as shown in Fig. 1-5. In each figure, the top triangle is assumed to have chirality +1. For edge sharing triangular lattice, in order to minimize total exchange energy, the neighboring triangle has to have chirality -1. As a result, the bottom triangle's spin configuration is uniquely determined. In contrast to this, for Kagomé lattice, the neighboring triangle has two choices, chirality +1 or chirality -1 with identical total minimized energies. The degeneracy is higher for Kagomé lattice. This is easy to understand. Since two neighboring triangles in Kagomé lattice only share one common spin, the upper triangle's spin configuration has less influence on the bottom one's compared to edge sharing triangle lattice in which two neighboring triangles share two common spins. Generally, the higher the degeneracy, the stronger the magnetic frustration.

Now, let's consider the entire triangular lattices in Fig. 1-6. For edge sharing triangular lattice (upper left), the only possible configuration consists of alternating chiralities, +1 and -1, from triangle to triangle. The structural unit cell is twice as large as a basic triangle. The magnetic unit cell is three times larger than structural unit cell. For Kagomé lattice, we can have either alternating chriality or uniform chirality. The upper right configuration has alternating chriality. The structural unit cell is as larger as eight basic triangles. The magnetic unit cell is three times larger than the structural unit cell. This state of Kagomé lattice with spins is called $\sqrt{3} \times \sqrt{3}$ state. If the chirality is uniform, then the structural unit cell and magnetic unit cell are identical. This uniform chirality

state is call q=0 state. The uniform chirality can be either +1 (bottom left) or -1 (bottom right).

For Kagomé lattice, zero energy mode exists in both q=0 state and $\sqrt{3}$ x $\sqrt{3}$ state. For $\sqrt{3}$ x $\sqrt{3}$ state, simultaneous rotation of all the spins on a hexagon as indicated by the upper right figure produces a zero energy mode. Similar zero energy modes can happen on any other hexagon on the Kagomé lattice. For q=0 state, both uniform +1 and -1 chirality, simultaneous rotation of all the spins along one straight line of spins as indicated in the bottom two figures produces a zero energy mode. Similar zero energy modes can happen on any other lines of spins. For these energy modes, the simultaneous rotation of spins maintains 120 degrees between adjacent spins. So there is no energy cost and the dispersion is flat at zero energy for all momentum. In contrast to Kagomé lattice, edge sharing triangular lattice does not support such zero energy mode.

Geometric magnetic frustration can be quantified. After measuring the magnetic susceptibility of an antiferromagnetic material, we can define the frustration as

$$F = \left| \frac{\Theta cw}{TN} \right| \tag{1.3}$$

where Θcw is the Curie-Wiess temperature from fitting the high temperature inverse magnetic susceptibility verses temperature and TN is the antiferromagnetic ordering temperature. In an ideal case without any frustration, f = 1. Conventionally, f > 10 is considered for strong magnetic frustration[1].

To sum up, compared to edge sharing triangular lattice, Kagomé spin lattice's ground state has a higher degeneracy from more choices on chirality distributions and zero

energy modes. Thus, Kagomé lattice is more frustrated magnetically and is more interesting for frustrated magnetism research.

1.2 Zn-paratacamite family

Zn-paratacamite minerals can be found naturally in Iran, Chile, United Kingdom and United States[12]. However, it has got its name since the Atacama Desert of northern Chile has the most abundant natural Zn-paratacamite minerals.

Zn-paratacamite has chemical formula $Zn_xCu_{4-x}(OH)_6Cl_2$. x varies between 0.33 and 1. When x=1, $ZnCu_3(OH)_6Cl_2$ is called herbertsmithite, named after mineralogist Dr. G.F Herbert Smith who worked for British Museum of Natural Histrory. In 1906, He discovered mineral paratacamite. Mineral herbertsmithite was first discovered in Chile, in 1972. Natural herbertsmithite has little value for laboratory research since they contains too much impurities. Nevertheless, the existence of such a mineral in natural proves that high purity sample can be synthesized in lab.

Fig. 1-7 shows herbertsmithite's structure with only Copper and Zinc. The Cu^{2+} ions form perfect Kagomé layers with Cu-Cu distance of 3.41Å. Zn^{2+} ions form layers right in the middle of two Cu^{2+} layers. Each Zinc ion is equal distance to six Cu ions. The distance between adjacent Cu layer and Zn layer is 2.34Å. The antiferromagnetic coupling between nearest Kagomé Cu spins comes from the Cu-O-Cu superexchange [13, 14, 15]. It is known that when the exchange angle is 180 degree, the interaction is strong antiferromagnetic. When the angle is 90 degree, the interaction is weak ferromagnetic. 97

degree separates ferromagnetism and antiferromagnetism for Cu-O-Cu superexchange. In herbertsmithite, this angle is 119 degree.

Zinc site in herbertsmithite can actually be occupied by either Cu or Zn[16]. The average Zn occupancy ranges from 0.33 to 1 for Zn-paratacamite. When it is all occupied by Zn, the mineral is herbertsmithite with x=1 for $Zn_xCu_{4-x}(OH)_6Cl_2$. As some Cu replaces Zn on interlayer Zn sites, x reduces from 1 and the mineral is generally referred as Zn-paratacamite. As long as the average occupancy of interlayer Zn sites are no less than 0.33, the crystal remains Rhomboheral and has space group $R\bar{3}m$.

Kagomé layers in herbertsmithite features ABC stacking as depicted in Fig. 1-8. Each unit cell consists of three Kagomé layers. Fig. 1-9 shows all the ions in one unit cell[17]. The hydrogen positions are determined by neutron powder scattering on deuterated sample $ZnCu_3(OD)_6Cl_2$.

It has been a long debate whether Zn exists on Cu site, based on thermodynamic data[18], magnetic susceptibility and magnetization[19], specific heat[20], NMR measurements[21, 22], powder neutron diffraction refinement[17, 20, 23] and other considerations[17, 24]. If Zn is stable on Cu site, $Zn_xCu_{4-x}(OH)_6Cl_2$ with x greater than 1 should exist. As discussed in chapter 3, this has been successfully achieved. Zn^{2+} has 28 electrons and Cu^{2+} has 27 electrons. Structure factor is proportional to the square of the number of electrons. It is very difficult to detect Zn^{2+} in the Kagomé layer by conventional X-ray since Cu^{2+} and Zn^{2+} has almost equal structure factors. However, synchrotron X-ray source with variable incident wavelength, such as Advanced Photon Source at Argonne National Laboratory in Chicago, can excel in this job. The incident wavelength can be tuned to Cu resonance edge such that Cu's structure factor diverges by

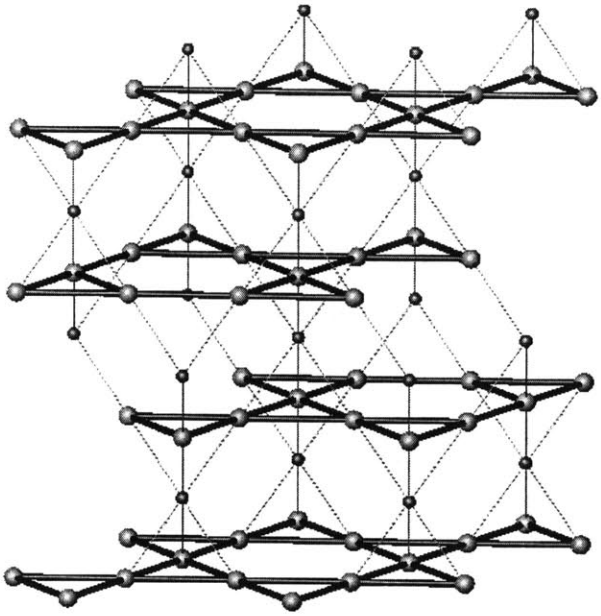

Figure 1-7: Structure of herbertsmithite with only Copper and Zinc. Copper is brown and Zinc is red. All nearest Cu-Cu bonds are equal and shown by strong black lines. All nearest Cu-Zn bonds are equal and shown by thin green lines.

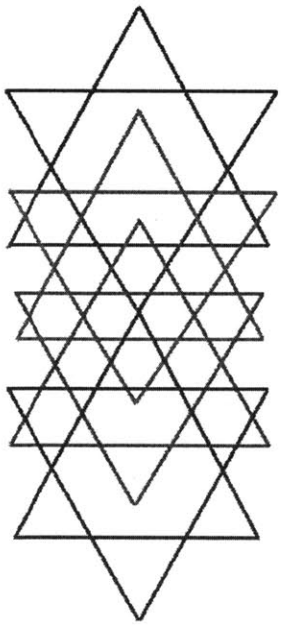

Figure 1-8: ABC stacking of kagomé layers in herbertsmithite. Such stacking is common for $R\bar{3}m$ space group. Different colors are for different kagomé layers.

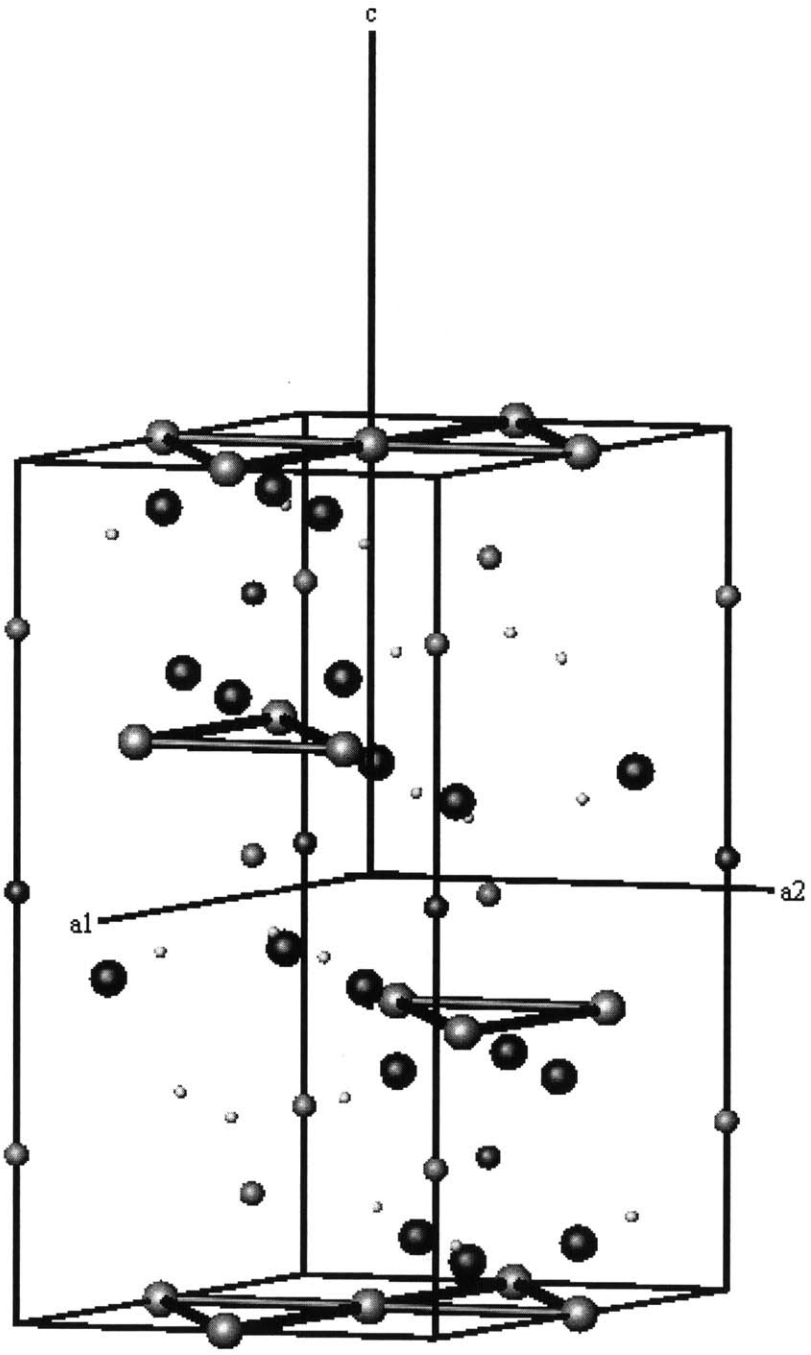

Figure 1-9: Rhombohedral unit cell structure of herbertsmithite, $ZnCu_3(OH)_6Cl_2$. Copper is brown, Zinc is red, Chlorine is green, Oxygen is blue and hydrogen is yellow. The Cu-Cu bond unveils a clear kagomé layer.

three orders of magnitude. In this case, essentially all the scatterings are from Cu ions. The same thing can be done for Zn. By analyzing the scattering intensities, the positions of Cu and Zn ions can be determined.

When x drops below 0.33, the crystals transforms to monoclinic and space group $P2_1/n$[17, 25, 26]. When x=0, all Zn are replaced by Cu and the mineral $Cu_2(OH)_3Cl$ is called clinoatacamite. Clinoatacamite consists of distorted Kagomé magnetic Cu layers separated by magnetic Cu layers. The triangle edges in Kagomé plane deviates about 0.2%. Powder clinoatacamite can be synthesized in laboratory[27].

A very important clarification has to be made here. In this thesis, $Zn_xCu_{4-x}(OH)_6Cl_2$ with x>0.80 is called herbertsmithite. This definition is less strict than the one used in mineralogy in which x has to be one. It is very hard to synthesis a sample with x precisely equal to one. Also, the most accurate characterization technique, the ICP, has an error of x-value around ±0.04. More importantly, with x>0.80, there is no magnetic transition down to 1.8K[28]. There should be no fundamental difference in the magnetic properties for x>0.8 samples. Actually, other mineral with the same chemical formula but different structure exists, such as kapellasite[29]. In this thesis, we are only interested in the herbertsmithite structure.

1.3 Synthesis of powder herbertsmithite

There are currently two methods to synthesis powder herbertsmithite. The first method is as follow[30]

$ZnCu_3(OH)_6Cl_2$. A 23 mL liner was charged with 0.66 g of $Cu_2(OH)_2CO_3$ (2.98 mmol), 0.31 g of $ZnCl_2$ (2.27 mmol), and 10 mL of water, capped and placed into a steel hydrothermal bomb under ambient room atmosphere. The tightened bomb was heated at a rate of 1 °C/min to 210 °C, which was maintained for 24 h. The oven was cooled to room temperature at a rate of 0.1 °C/min. A light blue powder was isolated from base of the liner by filtration, washed with deionized water, and dried in air to afford 0.80 g (94 %) of product. The powder gave an XRD pattern consistent with the Zn-paratacamite substructure (PDF 01-087-0679); no CuO was detected by XRD. Anal. Calcd. for $H_6Cu_3Cl_2O_6Zn$: H, 1.41; Cu, 44.44; Cl, 16.53; Zn, 15.24. Found: H, 1.42; Cu, 44.38; Cl, 16.46; Zn, 15.18.

The powder made using this method has been examined by chemical analysis and have x=1.00±0.04[30]. The structure has been check by X-ray diffraction which confirms the structure as herbertsmithite[30]. However, this method generates CO_2 as a byproduct which disturbs the growth environment. This disturbing prevents the formation of big single crystals. Also, CO_2 will increases the pressure inside the growth cell. As described below, this additional pressure makes this chemical reaction unsuitable for single crystal growth. The biggest single crystal made by this method has the size of roughly 0.04 mm^3 [30] which is way too small for magnetic measurement and neutron scattering.

Another method currently used to synthesis powder herbertsmithite starts with CuO, $ZnCl_2$ and water. The chemical reaction is,

$$3CuO + ZnCl_2 + 3H_2O \rightarrow ZnCu_3(OH)_6Cl_2$$

This method generates no gas which solves both problems from the previous method. What improves the growth environment more is that this reaction produces the same final product at a lower temperature (no more than 185°C) which further reduces the vapor pressure. Based on all these improvements, a single crystal growth technique has been invented.

1.4 Thesis Outline

This thesis discusses about single crystal growth for herbertsmthite and its characterization. Herbertsmithite is the first realized structurally perfect two-dimensional Kagomé antiferromagnet. Our group has successfully produced the first sufficiently big single crystal for neutron scattering. High quality crystals, ranging from 10μg to 200mg are ready for research.

Chapter 2 talks about the major instruments used, including three zone furnaces for crystal growth, inductive coupled plasma (ICP) for chemical analysis, SQUID for magnetic measurement and neutron triple axis spectrometer for bulk quality check.

Chapter 3 talks about the details of crystal growth technique. The reasons for the need of single crystal and possible future improvements have also been discussed.

Chapter 4 talks about the characterization for the crystals made. The linear chemical formula is determined by ICP. The structure is checked by single crystal X-ray diffraction

with the help of Dr. Peter Mueller from chemistry department at MIT. The mosaic is checked and the domain mass is measured by structural neutron scattering at NCNR NIST. The magnetic susceptibility is taken on SQUID. All the properties of the crystals have been compared with powder's. It is confirmed that high quality single crystal herbertsmithite has been synthesized.

Chapter 5 talks further about the defects of current crystals growth. The tricks of coaligning several crystals for neutron scattering experiment are discussed. At the end, we look ahead for possible future experiments on the crystals made available.

Chapter 2

Experimental Techniques

Three zone furnaces are available in Lee group at physics department at MIT. ICP and SQUID are provided by the Center of Material Science and Engineering at MIT. Neutron scattering facilities are at the NCNR NIST, Maryland.

2.1 Three zone furnace

Commercial three zone furnaces are purchased from Thermcraft Inc. The original outer reflective coated tubings, which help raising the temperatures inside, are replaced by a transparent one for in-situ observation. Each zone is approximately 15cm long and is heated and controlled independently. Two K-type thermocouples are deployed in each zone, one for temperature control and one for temperature high limit.

Proportional–integral–derivative controllers (PID controllers) are utilized for temperature control. PID loop calculate the power input based on the temperature

difference between present temperature and the set point. Three parameters for P, I and D can and should be tuned to optimize performance.

2.2 Inductive Coupled Plasma (ICP)

ICP measures the average ion concentration in a sample. After dissolving sample into 2% w/w HNO_3, as shown in Fig. 2-1, ICP sucks solution and sprays it into the middle of the inductive coils. The inductive coil produces a fast oscillating EM field which heats the solution and turns it into plasma state. The emission spectrum from the sample ions is captured by an optical grating and the intensity of specific wavelength characteristic of the particular element is measured. By comparing the measured intensity and the reference intensity, the concentration of the corresponding ion can be determined. To set the reference intensity, ICP needs to be calibrated using standard solutions each time before use.

There are some issues to pay attention for ICP measurement. First, single crystal is much better than powder in terms of higher precision. There may be some contamination in the powder sample, such as residual raw material. Single crystal is much easier to clean. It is also easy to check under microscope whether there are any contaminations left. Second, if the powder sample is a mixture of two or more phases, ICP can only tell the average ions concentrations. Single crystal is expected to be just one phase. During measurement, keep everything as stationary as possible. Do not cause any wind or walk around the equipment. Avoid windy days since the wind will affect the exhaust and

consequently the gas flux inside the plasma coil. The pump tube is very narrow. Make sure it does not touch the bottom of the vial since this may increase the impedance for solution flow. If a hardware condition has changed, such as the needle valve of the argon gas, calibration needs to be redone. If the machine shut down accidental, calibration need to be redone since the grating's gears have backslash errors.

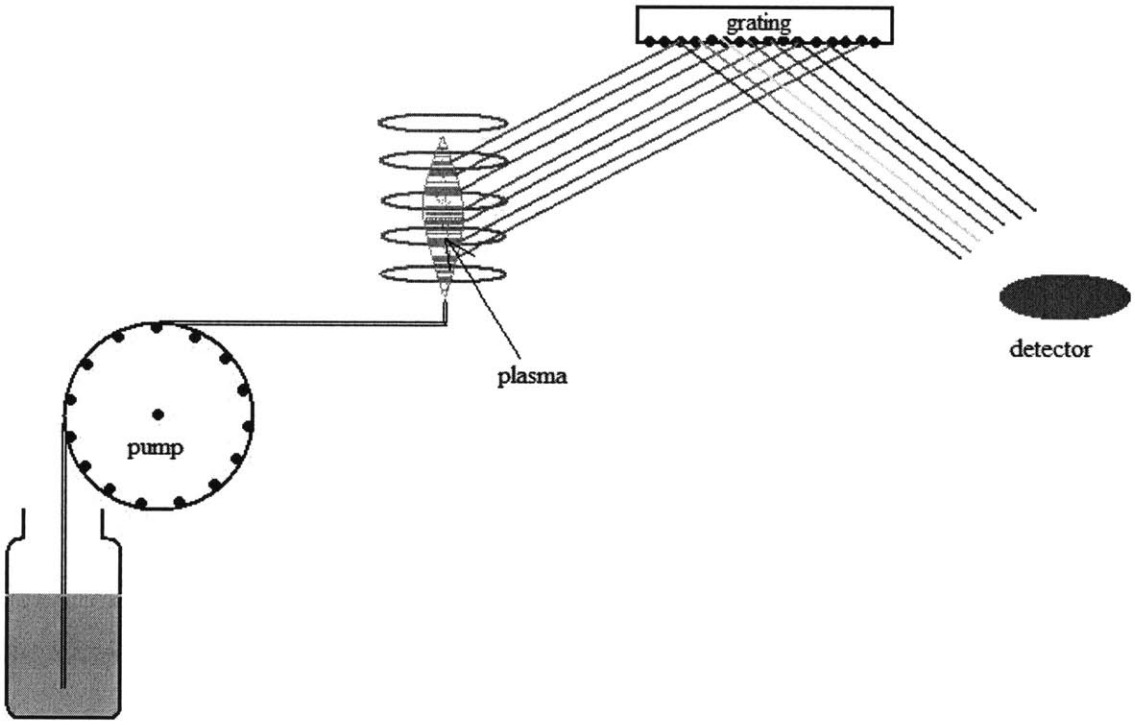

Figure 2-1: Schematic of inductive coupled plasma (ICP)

2.3 SQUID

Superconducting Quautum Interference Device from quantum design is used for magnetic property determination. The core is two superconductors separated by two thin insulating layers. The SQUID can detect very small magnetic field down to 10^{-14} Tesla. Strong magnetic field, up to 5T in ours, can be produced from a superconducting coil fully immersed in liquid helium bath at 4.2K.

Although the SQUID accuracy is far beyond needed for this thesis, in practice, its accuracy is greatly reduced by the background complication. Plastic straw, same as what people use to enjoy soft drinks, is used as sample holder. Below 0.1T, these plastic straws have a small ferromagnetic momentum due to impurities[28]. Beyond 0.1T, this small ferromagnetic saturation is overwhelmed by a diamagnetic magnetic momentum which increases as magnetic field increases[28]. For ferromagnetic sample, the sample's signal is dominant. It is not a big deal to ignore this background. However, for antifierromagnetic herbertsmithite, the background can be as large as the signal from a sample of several hundred micrograms. We can measure the sample holder's background and subtract it from the total signal. Although this method should work, to reduce the background signal contamination, the best way is to use a larger sample, preferably greater than 50mg.

All the data in this thesis are taken during warming up. There are two modes for magnetic moment measurement, sweep mode and settle mode. Sweep mode has a preset (may not be well maintained) temperature warming up rate and data is taken at predetermined time intervals. This mode is useful for magnetic transition temperature determination since the temperature never oscillates. However, the SQUID switches cooling mechanism at around 4K. Around 4K, SQUID cannot maintain the preset

warming up rate. As a result, there will be lags for temperatures. Settle mode overshoots the temperature and comes back to the target settle point before data is taken. This solves the temperature lag problem. However, since the temperature oscillates somewhat, this mode is not good for precise determination of magnetic transition.

2.4 Neutron Source and Triple Axis Spectrometer

One very popular source of neutron is located at the NIST Center for Neutron Research at Gaithersburg, Maryland, USA. Another popular source is at Oak Ridge National Laboratory, Tennessee. For this thesis, the work has been performed at NCNR NIST.

At NCNR NIST, there are two kinds of neutrons, thermal neutrons and cold neutrons. Thermal neutron is generated from a research nuclear reactor directly. On the shielding around the reactor's core, there are a few holes, called beam tubes. Monochromator and collimator are installed in it. When the shutter opens, well collimated single wavelength neutron beam comes out. Since thermal neutron comes directly out of the reactor core, the flux is high. There are several neutron guides installed also, connecting the reactor core to some additional instruments relatively far away from the reactor. Between the nuclear reactor and the neutron guide is a huge bath of liquid hydrogen. Since hydrogen has a large incoherent scattering length of neutron, the strong interaction between hydrogens and neutrons cools the neutrons efficiently to roughly 20K. These are the cold neutrons. Cold neutrons have lower energies which help to improve the energy resolution.

A triple-axis spectrometer, shown in Fig 2-2, is essentially the same as a typical x-ray spectrometer. From monochromator to sample is the first axis. From sample to analyzer is the second axis. From analyzer to detector is the third axis. When choosing collimator, there is a trade off between momentum resolution and intensity. The narrower the collimation, the higher the momentum resolution but the lower the intensity. Compared to x-ray spectroscopy, scanning bragg peaks using neutrons has two major advantages. First, neutron has strong penetrating power. It can exam the whole bulk while x-ray only sees the surface. Second, neutron can see hydrogen while x-ray cannot since hydrogen ion has no electron. The biggest disadvantage of neutron is that neutron requires a much bigger sample than X-ray. Also, after putting sample into the neutron beam, the sample becomes radioactive. This prohibits the sample from other uses.

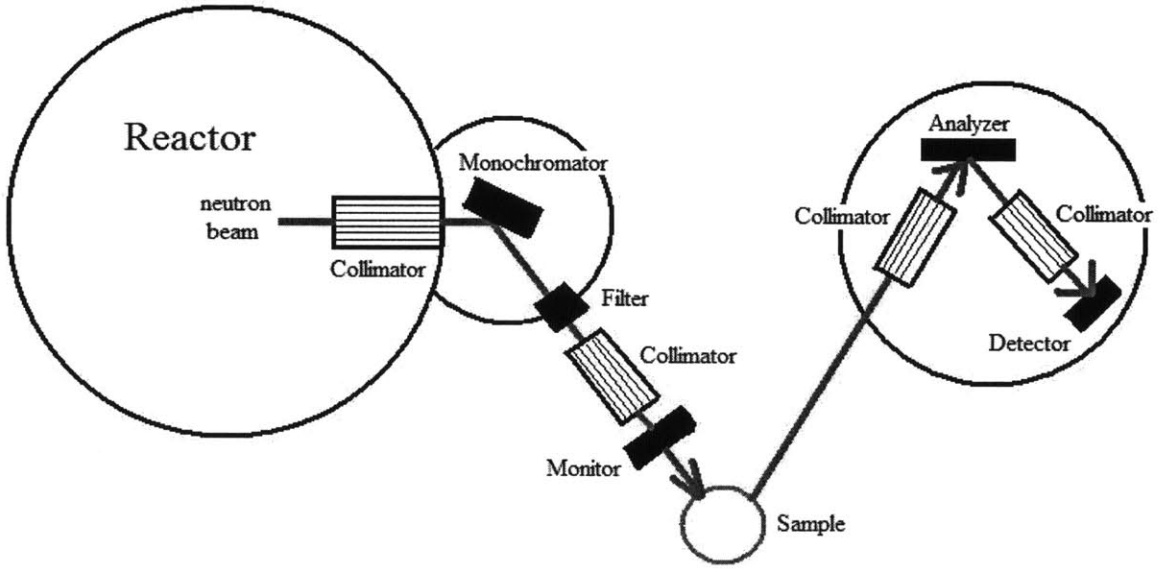

Figure 2-2: Schematic of a triple axis spectrometer

All sample holders for neutron scattering are made of aluminum. Aluminum has a very small neutron scattering cross section. So, it is almost transparent to neutrons. When taking data, keep in mind that the sample holder produces powder aluminum signal. It is crucial to subtract this and any other possible spurious signals.

Chapter 3

Herbertsmithite Single Crystal Growth

3.1 Motivation

The growth of single crystal herbertsmithite is vital for our understanding of spin liquid state. Although the experiment on powder sample was a big success, many questions still remain unveiled. For example, the anisotropy cannot be measured from powder sample. What are the magnetic susceptibilities for in Kagomé plane magnetic field and perpendicular-to-Kagomé plane field? What is the momentum dependence of neutron scattering intensities? Some new issues have also emerged, such as whether there is any magnetic impurity in herbertsmithite? Does the sample used for powder experiment indeed have Zn to Cu ratio as one to three? Many of these questions can be answered by measuring single crystal sample.

3.2 Crystal growth technique

Before growing big crystals, microcrystals have been grown under different conditions as a guide. From these trials, we know the proper starting material and the proper growth temperatures. These microcrystals, typically 0.5mm x 0.3mm x 0.3mm, can be used for x-ray diffractions.

First, commercial fused quartz tubing with a typical size of I.D. = 9mm and O.D. = 15mm is cut into pieces of 40cm long. One end of the fused quartz tubing is sealed using a hydrogen-oxygen torch. It is a good idea to wash the tubing as clean as possible, using pure water, acetone and sonic cleaner. Crystals tend to form onto tiny dusts. The less the tiny dusts are left in the tubing, the less the quantity of crystals will grow. A smaller number of crystals grown will increase the size of the products. After washing, high purity CuO, $ZnCl_2$ and deionized water are loaded into the tubing. After $ZnCl_2$ has been fully dissolved, the air inside the tubing is pumped out. The tubing is sealed about 6cm above the solution under vacuum. As a result, only saturated water vapor pressure is present in the fully sealed quartz tubing with all the raw material inside. Before growth starts, the tubing has been shaken vigorously and placed into a conventional furnace for both the purpose of pre-reactions and safety blast test at 185°C for 48 hours. Green fine powder herbertsmithite is formed during this process. After cooling down, put the powder herbertsmithite just formed to one end (zone 3) of the tubing and then place the tubing into three zone furnace horizontally, as shown in Fig 3-1.

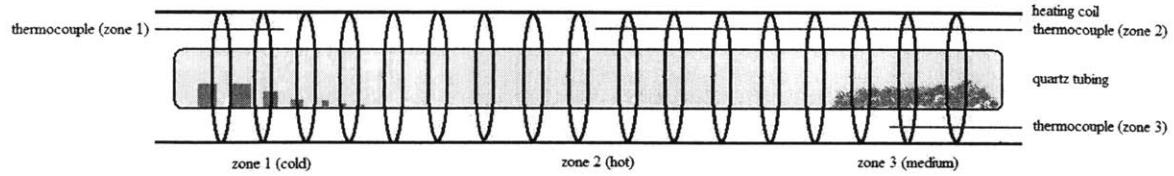

Figure 3-1: Schematic for herbertsmithite single crystal growth in three zone furnace. Zone 1 is for growth and zone 3 is for raw material. Zone 2 is used for growth control

Set the zone temperatures as T_1=180°C, T_2=160°C and T_3=140°C for 48 hours. This will clean up the growth zone. The color of the solution inside the tubing turns green, roughly like the one shown. After that set the temperatures as T_1=180°C, T_2=185°C, T_3=180°C. When temperatures get stabilized, slowly decrease T_1, preferably one degree every other day, until tiny crystals, preferably just one, appear in zone 1. To catch the first crystals grown, shoot light right into the growth zone and observe the region from all possible angles. Crystal has faces, so it only reflects lights strongly into a limited number of angles. Then hold T_1 until the end of crystal growth. Powder herbertsmithite will slowly dissolve into the solution and transport to the growth zone and crystallize. The temperature in the middle zone controls the temperatures gradient of the growth region. A greater temperature gradient will reduce the size of the growth zone. This will limit the total number of crystals grown and favor bigger crystal size. For current growth rate, typically, it takes 2 weeks to get $1mm^3$, 6 weeks to get $2mm^3$ and 4 months to get $3mm^3$.

Sometimes it may be necessary to increase the growth zone temperature a little bit after small crystals appear. This will limit the growth rate of the crystals which will improve the quality. Also, this reduces the possibility that a whole bunch of crystals appears later which will limit the size of the final products. Cameras have been setup to

take pictures of the growth region everyday. Close monitoring of the growth process gives hints how to adjust the temperatures.

This is the only method known which grows large single crystal herbersmithite. Other method, such as floating zone, does not work since herbersmithite has a decomposition temperature around 230°C, which is much lower than its melting point[28].

Different ratios of starting materials have been tried. The $ZnCl_2$ to CuO mole ratio ranges from 0.8 to 10 and the total mass of $ZnCl_2$ + CuO to water ratio ranges from 0.2 to 2. Different temperatures have also been tried other than the standard ones described above. However, the final products, $Zn_xCu_{4-x}(OH)_6Cl_2$, only have x ranges from 0.8 to 1. The only exceptions are for very low growth zone temperatures (equal or below 100°C). The details of the products are described in Chapter 4.

After the raw material is finished, the power is turned off. This ensures the fastest cooling rate possible. It takes roughly 2 hours to cool down to room temperature. Slow cooling is not preferred since small crystals of different phases will form onto the surfaces of the big crystals which reduce the quality of the bulk crystals. Even under the fast cooling process, some trace amount of contamination might also exist.

Some of my big crystals have cracks penetrating the bulk, as shown in Fig 3-2. The reason for their formation is still a question. One possibility is that some other phase of mineral is formed which has a different density from herbertsmithite. These cracks make the crystals relatively easy to fall apart. But it does not reduce the mosaic much as checked by elastic neutron scattering described in Chapter 4. This problem has not been seen in small crystals smaller than $1mm^3$. There are some tiny crystals resulted from the

cooling process on the surfaces. There is a smaller second domain at the back of the crystal.

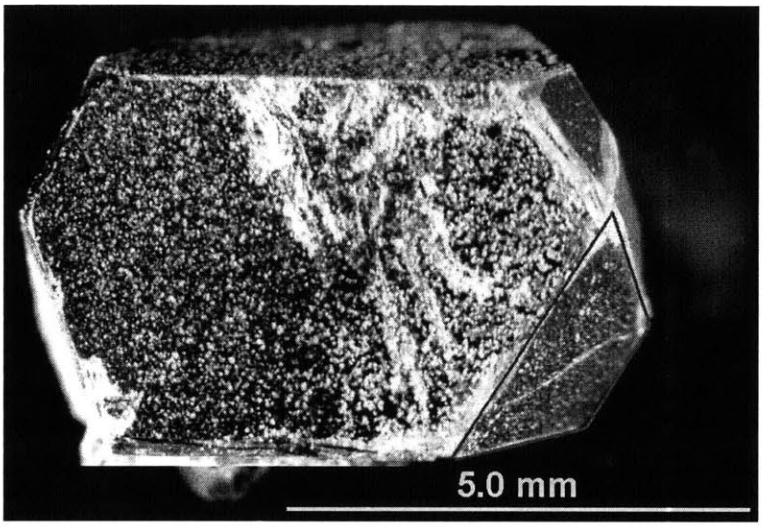

Figure 3-2: The biggest herbertsmithite ($Zn_{0.89}Cu_{3.11}(OH)_6Cl_2$) sample HTH_3_31 produced so far with approximate mass of 200mg. (0 0 1) face (Kagomé plane) is circled by red lines. Several apparent cracks penetrate the crystal bulk with unknown forming mechanism.

3.3 Improvements of growth technique

First, for magnetic neutron scattering[31], it is better to replace the hydrogen in the samples with deuterium. Deuterium has a much lower incoherent scattering cross section than hydrogen. This helps in reducing the background scattering. This is especially important when sign from the sample is weak. For magnetic excitations in spin liquid[5, 17, 32-43], a weak signal is often a problem. However, deuterium oxide's density,

1.107kg/m^3, is higher than water. After replacing water with heavy water in the raw materials, a higher density of the solution might make the deposition more difficult. As a result, a lower temperature of the growth zone is needed. As we lower the growth temperature, it might be the case that more crystals will form at the same time. This is not what we want. The growth of deuterated herbertsmithite is in progress now. What is observed so far confirms the educational guess.

Second, it might be a good idea to set up a cold point at the growth region. This cold end, hopefully, will have a very limited number of crystals grown right on top of it. If it works, this could solve the problem seen in the growth of deuterated herbertsmithite. One of my cooperators, Dr. Shaoyan Chu from the center of material science and engineering at MIT, has tried this idea[28]. He pumps cold water continues through a metal tube which has a small contact with the cold end of the sealed quartz tubing. However, he still gets more than a dozen crystals grow at the same time on top of the cold point. This is probably due to the reason that the thickness of quartz tubing makes the cold region inside the tubing much bigger than the contact point. One possible way to improve this is to use a thinner quartz tubing. However, thin quartz tubing may not survive the high pressure (about 10 atms). Another possible way is to drill a small hole through the quartz tubing and insert a small metal rod. This metal rod must not be chemically active with any of the chemical in the raw materials. Also, this metal should be sticky to melt quartz such that the drilled hole can be well sealed. The feasibilities of these ideas need further thoughts.

Third, this growth technique can be used to make other similar single crystal minerals, such as Mg-paratacamite and Gillardite[44, 45]. Recently, Mg version of

herbertsmithite gets a lot of attention. It is very similar to herbertsmithite. However, Mg^{2+} has only 10 electrons while Cu^{2+} has 27. So, Mg^{2+}'s structural factor is only roughly 14% of Cu^{2+}'s. It is much easier to tell whether Mg and Cu exchange places or not. This makes the analysis of many experimental data much less ambiguous. In general, as long as the raw powder dissolves into water, the solubility is sensitive to temperature, and the formation temperature is below 200°C, this growth technique can be used for crystal formation.

3.4 Summary

Powder sample loses all angular information. Also, data taken on powder sample is generally less reliable compared to single crystal's. Magnetic susceptibility has been measured on orientated herbertsmithite powder[46]. However, since high quality single crystal is available now, much better data will be there soon.

Currently, single crystal is synthesized by transporting ions in water solution inside sealed quartz tubing powered by a temperature gradient. However, to lower incoherent background for neutron scattering, future growth will replace water with heavy water. The growth process may be affected by this modification, despite water and heavy water are very similar. To get larger crystal, we can create a small cold point for condensation of ions. But this may not work well. Even it works, some technical details still need a lot of thoughts.

Our crystal growth method can be generalized. For example, we can make Mg-paratacamite or gillardite single crystals. Mg version of herbertsmithite might be a better material to work on since Mg^{2+} and Cu^{2+} have distinct structure factors. This helps a lot in eliminating some ambiguities for herbertsmithite.

Chapter 4

Characterization of Single Crystal Herbertsmithite

All crystals grown look very alike, green and crystal clear. Their green looks darker than powder sample simply due to the difference in grain sizes. Some big crystals beyond 30mg have cracks. The only exception is batch 45. These crystals look opaque and have slightly less regular shapes.

4.1 Chemical analysis

The average chemical formula of the crystals is checked by inductive coupled plasma (ICP). Since ICP irreversibly destroys the sample, several small single crystals are picked from the batch for measurement. These crystals are washed carefully using sonic cleaner and checked under microscope to make sure no significant contamination is sticking on. To prepare the solution for ICP, crystals are dissolved into 2% w/w HNO_3. The concentrations of Cu^{2+} and Zn^{2+} are calculated and controlled to be between 10 to 100ppm where ICP is most sensitive[28]. Several concentrations are made and the

average result is calculated. The standard solutions, preferably five or more, for ICP calibration are made with Cu^{2+} and Zn^{2+} concentrations spreading out a little bit wider than sample solutions'.

The results are summarized in Table 4-1. Sample column shows the name for each batch. Mean is the average x value in $Zn_xCu_{4-x}(OH)_6Cl_2$ obtained from ICP. N_{Zn}/N_{Cu} is the mole ratio of Zn^{2+} ions to Cu^{2+} ions in the starting material. Solid/H_2O is the mass ratio of total solid ($ZnCl_2$ and CuO) to H_2O in the starting material. Temperature column

Sample	Mean x	N_{Zn}/N_{Cu}	Solid/H_2O	Temperature	$100xN_{Zn}/N_{H2O}$	$100xN_{Cu}/N_{H2O}$
HTH_1_1	0.977	3/1	1/1.5	140/160/180	7.38	2.46
HTH_1_3	0.907	0.8/1	1/0.5	140/160/180	15.28	19.11
HTH_1_10	0.923	3/1	1/0.8	170/175/180	13.83	4.61
HTH_1_11	0.880	2/1	1/1.5	170/175/180	6.82	3.41
HTH_1_12	0.933	5/1	1/1	170/175/180	11.84	2.37
HTH_1_13	0.950	3/1	1/2	170/175/180	5.53	1.84
HTH_2_16R	1.121	1/1	1/1	100/140/180	8.35	8.35
HTH_2_21T	0.967	1/1	1/3	150/180/165	2.78	2.78
HTH_2_22R	0.917	4/1	1/1.5	150/180/165	7.69	1.92
HTH_2_23T	0.922	3/1	1/1	150/180/165	7.38	2.46
HTH_2_27	0.914	3/1	1/3	150/185/165	3.69	1.23
HTH_2_28	0.805	3/1	1/5	150/185/165	2.21	0.74
HTH_2_29	0.874	5/1	1/3	150/185/165	3.95	0.79
HTH_3_30	0.943	7/1	1/1.5	174/184/180	8.13	1.16
HTH_3_31	0.977	10/1	1/1.5	174/184/180	8.33	0.83
HTH_3_32	0.942	7	½	160/170/180	6.10	0.87
HTH_3_33	0.929	10	½	160/170/180	6.24	0.62
HTH_3_37	0.945	5	½	160/170/180	5.92	1.18
HTH_4_41	1.058	1	1	80/130/180	8.35	8.35
HTH_4_45	1.095	2.55	1	80/130/180	10.76	4.22

Table 4-1: ICP results summary

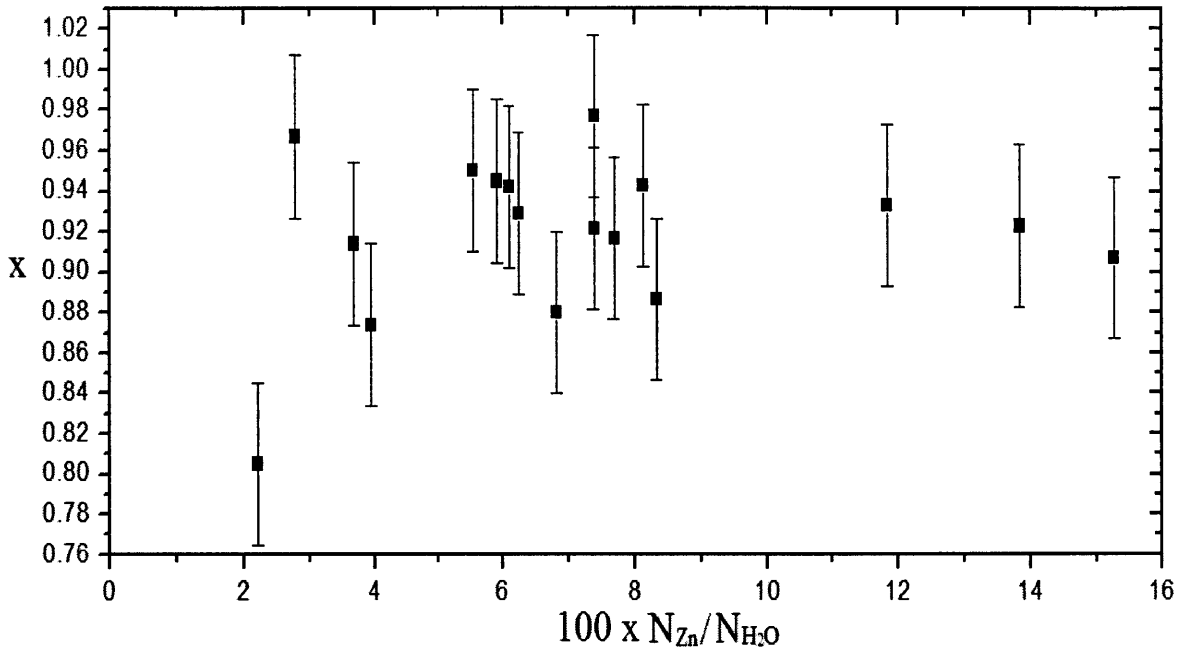

Figure 4-1: x value Vs $100xN_{Zn}/N_{H2O}$. Samples with growth region temperature smaller than 140°C are excluded.

gives the stable growth temperatures for each zone. $100xN_{Zn}/N_{H_2O}$ column gives the mole ratio of Zn^{2+} ions to H_2O molecules in the starting material multiplied by 100. $100xN_{Cu}/N_{H2O}$ column gives the mole ratio of Cu^{2+} ions to H_2O molecules in the starting material multiplied by 100.

Theoretically, for $100xN_{Zn}/N_{H2O}$, a very high value and a very low value should both give relatively low x. This can be easily explained. For very low N_{Zn}/N_{H2O}, the overall Zn^{2+} ion concentration in the starting material is low. This reduces the Zn^{2+} ion concentration in the final product. For very high N_{Zn}/N_{H2O}, the solution becomes very acidic. High acidity dissolves more CuO and increases the Cu^{2+} ion concentration in the growth environment. This also reduces the Zn^{2+} ion concentration in the final product. However, this is not the case despite that $100xN_{Zn}/N_{H2O}$ varies almost by a factor of ten

as clearly seen in Fig 4-1. The error of x-value measured by ICP is about ±0.04. Within error, the final product all have x value close to 1 and roughly the same. This indicates the final product is a line compound.

Interestingly, a very low growth temperature (cold zone temperature), equal or below 100°C, gives x-value greater than 1 (samples HTH_2_16R, HTH_4_41 and HTH_4_45). This is a surprise. It is believed that a higher growth temperature will favor Zn-Cu site mixture[17]. As a result, samples with x greater than one should be produced at a higher than normal temperature.

4.2 Structure determination

The structures of the crystals are determined by single crystal X-ray diffraction. The samples for this measurement typically have the size of $0.2mm^3$ due to X-ray's low penetrating power. Single domain samples are selected using optical polarizations.

Crystals grown under the condition mentioned above have herbertsmithite structure as previously reported, including $Zn_{1.06}Cu_{2.94}(OH)_6Cl_2$. However, for $Zn_{1.10}Cu_{2.90}(OH)_6Cl_2$, it is very hard to find a high quality single crystal, even for a size of $0.1mm^3$. The detailed X-ray diffraction result for HTH_1_11 is included in Appendix A. The detailed X-ray diffraction result of HTH_4_41 is included in Appendix B. A brief summary of the results is in Table 4-2.

Empirical formula*	$Zn_{0.88}Cu_{3.12}(OH)_6Cl_2$	$Zn_{1.06}Cu_{2.94}(OH)_6Cl_2$
Crystal system	Rhomboheral	Rhomboheral
Space group	$R\bar{3}m$	$R\bar{3}m$
a	6.8345(9) Å	6.8300(12) Å
b	6.8345(9) Å	6.8300(12) Å
c	14.0538(19) Å	14.049(3) Å
α	90	90
β	90	90
γ	120	120
Volume	568.51(13) $Å^3$	567.57(17) $Å^3$

Table 4-2: Crystallographic data for herbertsmithite determined by single crystal X-ray diffraction at 100K. *: ICP results.

It is possible to determine crystal orientation from the shape. All the big sides on a bar shaped herbertsmithite crystal are (1 0 1) faces. This is confirmed by x-ray diffraction on more than 10 crystals. Fig 4-2(a) shows a typical bar shaped crystal. When you look at this crystal, the faces BCED is (1 0 1). Then you can measure angle DBC. If it is 124 degrees, then face ABC is likely to be (0 0 1). If you look at the same crystal from the other side as shown in Fig 4-2(b), a similar face HIJ is there but smaller. Angle KIJ is also roughly 124 degrees. Empirically, the bigger face ABC is the (0 0 1) face. If you look down perpendicularly at face ABC, it should be an equal lateral triangle. Detailed measurement, either by X-ray or Neutron, must be done to be certain for the crystal orientation. However, knowing this empirical determination method can make the

measurement much easier. The left end of the crystal does not have well defined faces. This is the root from which the crystal has grown.

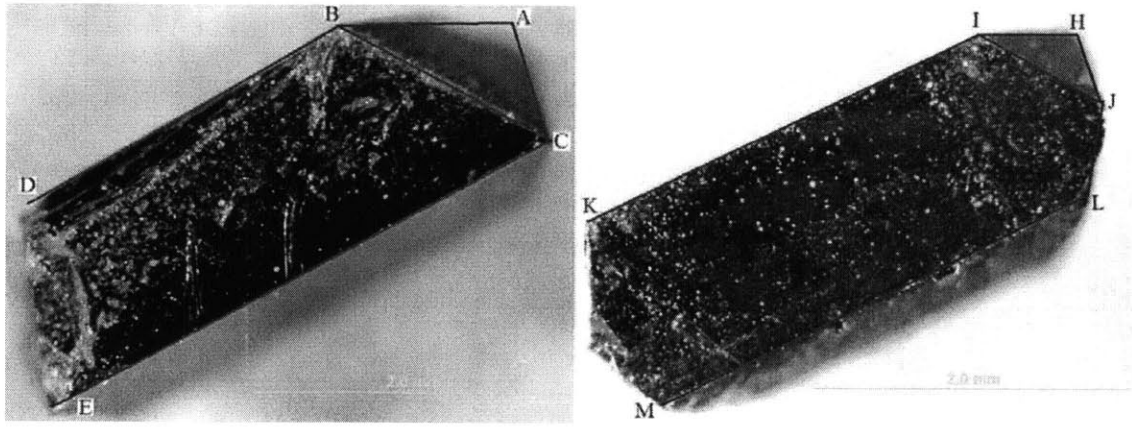

(a) (b)

Figure 4-2: (a) and (b) show the same crystal. (b) is obtained from rotating (a) with respect to CE by 180 degrees. Face BCED is the opposite parallel face of face IJLMK.

The empirical orientation determination can be explained with the crystal structure. Fig 4-3 shows all the (1 0 1) faces for herbertsmithite, with a, b and c axis labeled. There are in total twelve (1 0 1) faces. As crystal grows, eight of the twelve faces grow much larger. The rest four faces, ABG, ADE, HDE and HBG, finally disappear. Now the crystal becomes octahedral. Lots of octahedral shaped tiny crystals, roughly $0.2mm^3$, are produced. As growth continues, four out of eight faces, AJC, AJF, CHI and FHI, grow very big and become the four side (1 0 1) faces of a bar shaped crystal. Face FJCI, the Kagomé plane, shows up at the end of the bar shaped crystal. Purely based on geometric analysis of crystal structure, there can be other growth process producing differently shaped crystal with different face indices. However, from the observation of dozens of

crystals, the process described above is the only one happened so far. Relevant angles are calculated and compared with observed ones. These angles are useful for crystal alignment for neutron scattering.

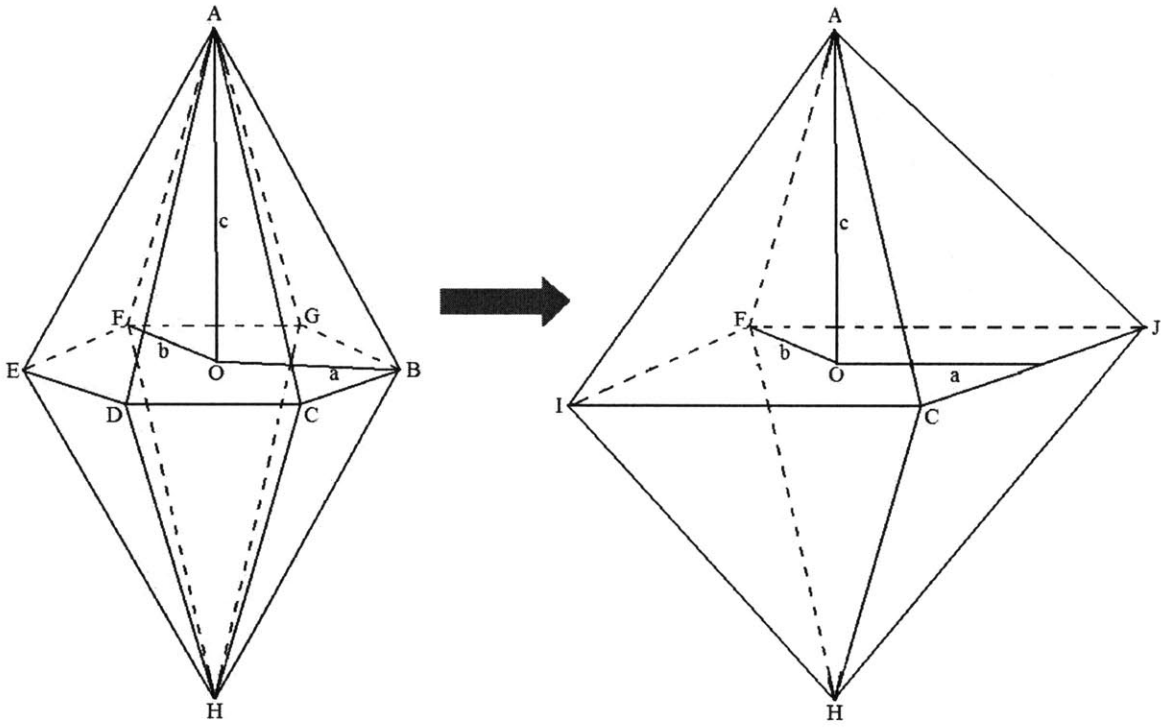

Figure 4-3: Left: crystal structure of herbertsmithite. There are twelve (1 0 1) faces.

Right: the crystal reduces to octahedral as four faces disappear during growth.

$\angle$AJC = $\angle$AJF = 56.1°. Angle between OA and face AJC: $\angle$OA-AJC = 22.8°.

4.3 Structural Neutron Scattering Measurement

The biggest sample produced so far, HTH_3_31, has been shown in Fig 3-2. It has total mass of roughly 230mg and well shaped crystal faces. Due to the neutrality of charge and

heavy mass (almost 2000 times heavier than electron), neutron has strong penetrating power and is ideal to examine the quality and property for the bulk.

The target plane of atoms, Kagomé plane in our case, needs to be aligned horizontally since neutron triple axis spectrometer at NIST has horizontal scattering plane. Here is how to align the sample. The biggest face of HTH_3_31, the face we are looking right into in Fig 3-2., is (1 0 1). This face is laid down horizontally. From the geometry of the crystal structure, (-1 2 0) is perpendicular to (1 0 1). So in reciprocal space, (-1 2 0) is pointing horizontally. After fixing two-theta angle at the value for (-1 2 0) bragg peak, rotate theta and look for bragg peak. Then, the sample is rotated with respect to (-1 2 0) direction by 67 degrees such that the (0 0 1) face will be flat. Then the crystal should be well aligned after some minor adjustment. Although any directions 60 degrees apart in the Kagomé plane are equivalent, due to the absorption effect, the strongest (-1 2 0) peak is selected, both for the mass determination purpose (described below) and for any further measurement.

The measurement was conducted on Spin Polarized Triple Axis Spectrometer in the guide hall of NCNR NIST, Maryland. The configuration of the instrument was monochromator - 80 minute collimation - sample – Be filter -80 minute collimation -3 flat blade analyzer-detector. First, a smaller sample of mass 15.800mg was aligned and its (-1 2 0) bragg peak intensity was measured to be 1400 count/second. The same measurement was done on HTH_3_31. The intensity of (-1 2 0) peak was 12000 count/second. From the ratio of the intensities, the mass of HTH_3_31 is roughly 135mg. Taking the larger absorption effect of bigger sample in consideration and also by looking

at the size of the second domain on the back of HTH_3_31, a good guess for the mass of the bigger domain of HTH_3_31 would be 200mg.

To check the mosaic of the crystal, theta scan at fixed 2-theta angle has been performed on peak (-1 2 0) and the result is shown in Fig 4-4. The width of the peak is roughly 80 minutes. This means that our sample has a mosaic equal or smaller than the instrument's resolution.

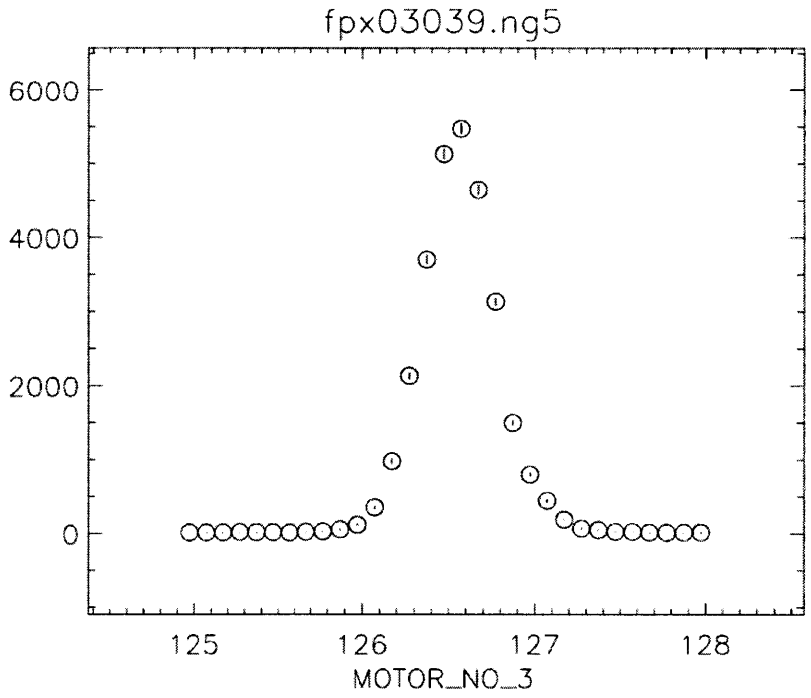

Figure 4-4: Theta scan on HTH_3_31's (-1 2 0) bragg peak. The horizontal scale is theta angle in degree. The absolute degree value has no meaning. The vertical scale is count/second.

4.4 Magnetic property

To be surer about the property of the final product, magnetic susceptibility has been measured for microcrystals and big unoriented crystals. As expected for $0.8 < x < 1$ Zn-paratacamites, none of our samples in this x range has magnetic transition down to 1.8K. The Curie-Wiess temperature is determined by fitting the inverse magnetic susceptibility data above 150K.

Magnetic measurements on newly grown microcrystals are measured using SQUID. The average crystal size in the sample collection is $0.2mm^3$. For example, 231.6mg of HTH_1_1 was sealed into the straw. HTH_1_1 has formula $Zn_{0.98}Cu_{3.02}(OH)_6Cl_2$ from ICP measurement. Comparing the crystal size and the total amount of sample, the signal should be just a powder average.

In Fig 4-5, the measurement for HTH-1-1 is compared with MPS-6-135[47]. MPS-6-135 is made by Nocera's group and its magnetic susceptibility data taken by Dr. Joel S. Helton is used as a benchmark for the property of herbertsmithite. MPS-6-135 is claimed to have formula $ZnCu_3(OH)_6Cl_2$[47]. However, some doubt it as $Zn_{0.93}Cu_{3.07}(OH)_6Cl_2$[17, 20, 23]. MPS-6-135 is real powder with micrometer sized grains. It may hide some contamination which has not been washed away. In contrast to that, HTH_1_1's big grain sizes made the contamination easy to wash. Under microscope, washed crystals looked very clean. Thus, HTH_1_1's x-value from chemical analysis is more reliable. For the comparison of results, the signals from those two independently made samples basically collapse onto the same curve.

In Fig 4-6, the inverse magnetic susceptibility is plotted versus temperature. By fitting the high temperature part, the g factor and Curie-Wises temperature is determined. The g factor is 2.348, compared to 2.464 for MPS-6-135. The Curie-Wiess temperature is

291.0K compared to 298.2K of MPS-6-135. The deviations between two samples are typical and tolerateable from the experience of powder measurements done before.

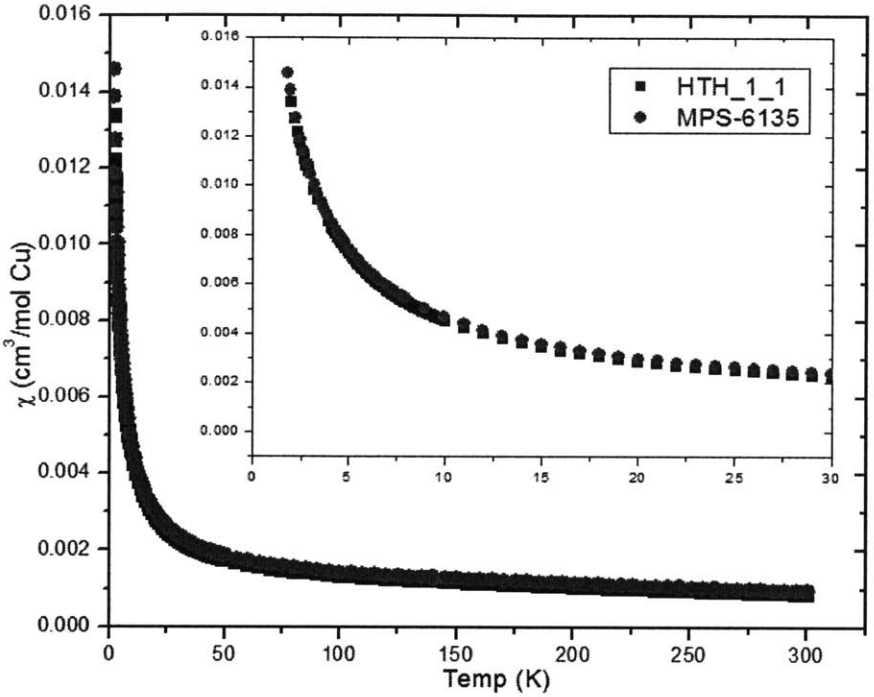

Figure 4-5: Magnetic susceptibility of HTH-1-1 and MPS-6-135

Insert: same plot zoomed in for temperature below 30K

In Fig 4-7, the zero-field-cool data and 500Oe-field-cool data are compared. For ZFC, the sample was cooled from 300K down to 2K under zero magnetic field. For 500Oe FC, the sample was cooled from 300K down to 2K under 500Oe magnetic field. Each data set was measured by warming up from 2K. From both previous theoretical predictions[48-54] and previous measurement on MPS-6-135, those two curves should show no difference. This is what has been observed. The gap around 4K is due to effect of sweeping mode.

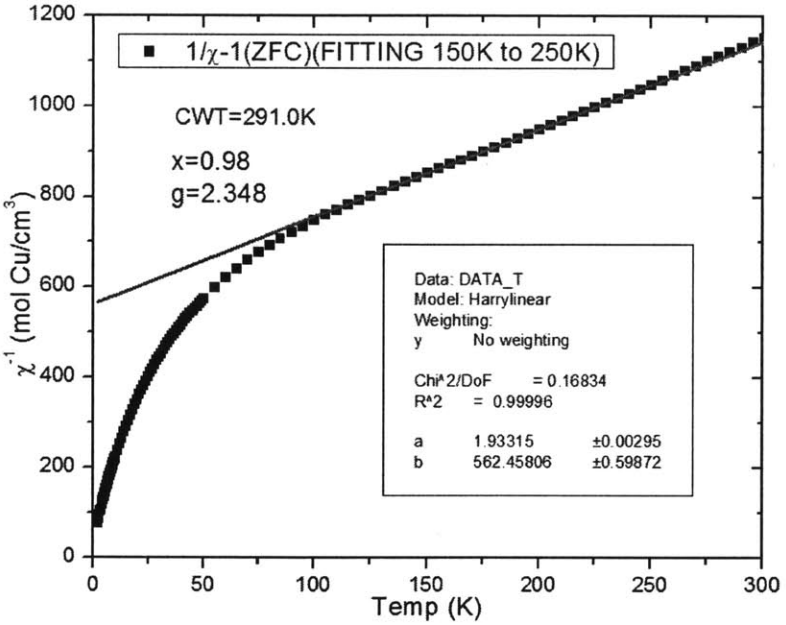

Figure 4-6: Inverse magnetic susceptibility fitting for HTH_1_1

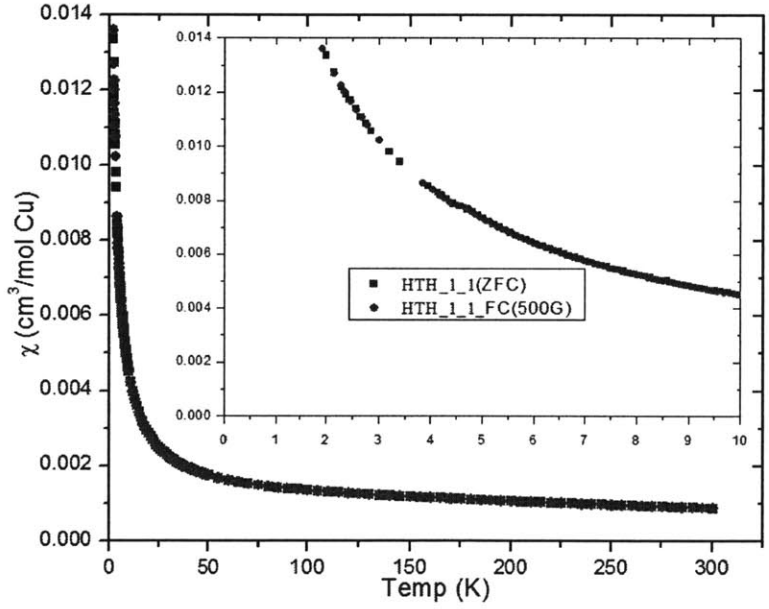

Figure 4-7: Field cool and zero field cool magnetic susceptibility of HTH_1_1. The insert is the same data zoomed in for low temperature.

4.5 Summary

The Zn to Cu ratios have been checked for every batch of crystals made. With starting materials consisting of only $ZnCl_2$, CuO and water, x-value ranges from 0.805 to 1.121. Herbertsmithite is possibly a line compound since x-value is relatively stable while the growth environment changes dramatically. Three samples have x-value greater than 1. They all have cold end temperatures (growth temperatures) equal or less than 100°C.

More than one structure can have the same linear chemical formula. To make sure our crystals do have the Zn-paratacamite structure, single crystal x-ray spectrometry has been performed. The results of two representative batches, one with $x<1$ and one with $x>1$, are discussed with full reports attached in the Appendix.

Due to the strong penetrating power, the bulk qualities of crystals are examined by structural neutron scattering experiment at NCNR NIST. The mosaics are under the instrument's resolution of 80 min. For slow crystal growth in water solution, this is not a surprise. Other methods, such as floating zone, often result in larger sample mosaic. The dominant domain of the biggest single crystal, HTH_3_31, has a mass of roughly 200mg. This should be big enough for further magnetic neutron scattering measurement although bigger sample is highly preferred.

At last, magnetic susceptibilities have been measured. None of the samples with $x<1$ has magnetic ordering down to 1.8K. The result for HTH_1_1 is shown and compared with previous powder data. No material difference has been found. For samples with $x>1$, this is not the case. Study for these samples is still in progress.

Every measurement confirms that high quality single crystal herbertsmithite has been

successfully synthesized using a distinct approach than previously reported[30]. This paves the road leading to further research on frustrated magnetic systems.

Chapter 5

Discussion

5.1 Problems on current crystal growth

Although the crystal growth has been a success, some issues still need to be discussed.

First, the growth rate is too slow. Right now, it takes half year to get a crystal bigger than 200mg. Any attempt to grow faster results in an increment of crystal number and a reduction of crystal size. Dr. Shaoyan Chu has added $CuCl_2$ to the raw material[28]. The growth rate did not change much. However, the final product was $Zn_{0.33}Cu_{3.67}(OH)_6Cl_2$. This is because more Cu is provided which increases the Cu concentration in the final product.

Second, the size of the crystal is limited by the size of the quartz tubing. The size of the quartz tubing is limited by the pressure needed for the growth. For a certain thickness, the larger the radius, the lower the pressure the tubing can stand. The biggest tubing used up to now has inner diameter of 9mm. For commercial available tubing, the biggest feasible one has inner diameter of 13mm. This cross section is twice as large as the one used. Although the raw material can be doubled, the area of the growth region is also

enlarged. This may not help much in improving the size of the crystal. For neutron scattering, the larger the sample the better since magnetic signal from herbertsmithite is likely to be very weak. New idea of crystal growth needs to be invented if 500mg or larger sample is necessary.

Third, the cracks in big samples remain a problem. Although these cracks do not reduce the mosaics of the samples or divide the crystals into domains, they make the samples very fragile. Herbertsmithite is very soft and brittle. Handling cracked samples are quite difficult and risky. It is crucial to understand why these cracks only happen in samples bigger than $2mm^3$. Amazingly, one batch, HTH_3_37, has a much better quality than all other batches. Several largest crystals in this batch have size between $1mm^3$ to $2mm^3$. They look just like clearly cut jewelry gems. The sharpness of their shape and the clarity are by far the best.

5.2 Coaligning crystals

Neutron scattering needs big sample. If the sample size cannot be improved easily, coaligning several single crystals is not a bad idea. The best coaligning idea is putting several well shaped crystals side by side onto a flat aluminum sample holder. Three faces are needed for each crystal, preferably two side intersecting (1 0 1) faces and one (0 0 1) face intersecting both of them. The coaligning method is shown in Fig 5-1. Opposite (1 0 1) faces on the sides are parallel. The bottom (1 0 1) faces are placed against flat sample holder. Another pair of (1 0 1) faces are placed against each other. With two

pairs of faces coaligned, each crystal still has two orientations. For each crystal, choose the orientation which makes (0 0 1) faces parallel to each other. Thus, the two crystals are well coaligned. Since hydrogen has a large incoherent scattering cross section and most, if not all, glues contain hydrogen, gluing them together is not the preferred method. The best way is to wrap the samples with aluminum foils. This method has the lowest possible background. If the sample cannot be well fixed in place, fomblin is a possible solution. Fomblin has linear formula $CF_3O[-CF(CF_3)CF_2O-]_x(-CF_2O-)_yCF_3$. It does not contain any hydrogen and is very sticky at room temperature. At helium temperature, it freezes.

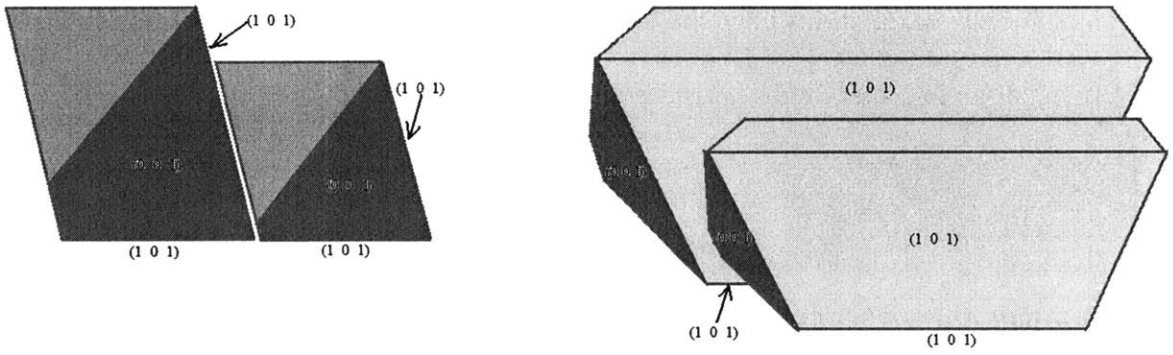

Figure 5-1: Crystal coaligning. The faces used for coaligning has been labeled. The right figure is the side view looking to the right of the left figure.

5.3 **Future studies of single crystal herbertsmithite**

Other than the Heisenburg exchange interaction, Dzyaloshinskii-Moriya interaction[55-57] is also believed to exist. Effects of DM interaction have been

calculated[58-61], such as magnetic anisotropy. However, the magnitude of DM interaction is unknown. By measuring the magnetic susceptibility with magnetic field along different directions, a better understanding of the DM interaction can be obtained.

Heat capacity measurement can also be performed on single crystal with magnetic field along different directions. For each magnetic field orientation, specific heat data can be taken against temperature at different field magnitudes. This helps in deepening our understanding of the crystal.

Magnetic neutron scattering can be done on our biggest single crystal, HTH_3_31. Dispersion of the low energy inelastic excitations along high-symmetry directions of the two dimensional Brillioun zone can be measured. It is also interesting to find the Q-vectors where the excitations have the lowest energies (or are gapless). It is good to know the effects of an in-plane field versus an out-of-plane field.

5.4 Summary

No one knows how big a sample is needed for magnetic neutron scattering. As long as the sample can be fully penetrated by neutron beams, the bigger the better. Our 200mg sample is probably the minimum required. Simply using bigger quartz tubing may or may not help. Theoretically, coaligning several crystals can solve this problem. However, it is not a very easy job to maintain the mosaic.

Small size is not the only hurdle. The growth cycle now is about half a year. This is too slow to efficiently implement any improvement idea. This slowness also limits the

total number of big crystals available. Right now, there is a trade off between the size of the crystals and the growth rate. Another problem is the cracks in the big crystals. Although these cracks do not deteriorate the quality of the crystal as far as we know, they made the crystals fragile.

Due to the active theoretical researches on herbertsmithite and the exciting powder data, further experiments on single crystal sample have already been planned. These measurements include magnetic anisotropy, heat capacity anisotropy and magnetic neutron scattering. All these will help a lot to further our understanding of frustrated magnetism.

Bibliography

[1] A. P. Ramirez, *Annual review of Materials Science* **24**, 453 (1994)
[2] H. T. Diep, editor, *Frustrated Spin Systems*, World Scientific, Singapore, 2004
[3] P. W. Anderson, *Materials Research Bulletin* **8**, 153 (1973)
[4] P. W. Anderson, *Science* **235**, 1196 (1987)
[5] J. S. Helton, K. Matan, M. P. Shores, E. A. Nytko, B. M. Bartlett, Y. Yoshida, Y. Takano, A. Suslov, Y. Qiu, J.-H. Chung, D. G. Nocera, and Y. S. Lee, *Physical Review Letter* **98**, 107204 (2007)
[6] J. H. Van Vleck, *Journal of Chemical Physics* **9**, 85 (1941)
[7] L. Neel, "Magnetism and the Local Molecular Field", Nobel Prize Lecture, 1970.
[8] A. Yoshimori, *Journal of the Physical Society of Japan* **14**, 807 (1959)
[9] R. Liebmann, *Statistical Mechanics of Periodic Frustrated Ising Systems,* Springer-Verlag, Berlin, 1986
[10] J. Villain, *Journal of Physics C: Solid State Physics* **10**, 4793 (1977)
[11] I. Syôzi, *Progress of Theoretical Physics* **6**, 306 (1951)
[12] J. L. Jambor, J. E. Dutrizac, A. C. Roberts, J. D. Grice, and J. T. Szymanski, *Canadian Mineralogist* **34**, 61 (1996)
[13] P. W. Anderson, *Physical Review* **79**, 350 (1950)
[14] P. W. Anderson, *Physical Review* **115**, 2 (1959)
[15] K. P. Sinha and N. Kumar, *Interactions in Magnetically Ordered Solids,* Oxford University Press, Oxford, 1980.
[16] R. S. W. Braithwaite, K. Mereiter, W. H. Paar, and A. M. Clark, *Mineralogical magazine* **68**, 527 (2004).
[17] J. Helton, *The Ground State of the Spin-1/2 Kagomé Lattice Antiferromagnet: Neutron Scattering Studies of the Zinc-Paratacamite Mineral Family,* PhD thesis, Masasachusetts Institute of technology, 2009.
[18] G. Misguich and P. Sindzingre, *European Physical Journal B* **59**, 305 (2007)
[19] F. Bert, S. Nakamae, L. Ladieu, D. L'Hôte, P. Bonville, F. Duc, J.-C. Trombe, and P. Mendels, *Physical Review B* **76**, 132411 (2007)
[20] M. A. deVries, K. V. Kamenev, w. A. Kockelmann, J. Sanchez-Benitez, and A. Harrison, *Physical Review Letters* **100**, 157205 (2008).
[21] T. Imai, E. A. Nytko, B. M. Bartlett, M. P. Shores, and D. G. Nocera, *Physical Review Letters* **100**, 2077203 (2008).
[22] A. Olariu, P. Mendels, F. Bert, F. Duc, J. C. Trombe, M. A. deVries, and A. Harrison, *Physical Review Letters* **100**, 087202 (2008).
[23] S.-H. Lee, H. Kikuchi, Y. Qiu, B. lake, Q. Huang, K. Habicht, and K. iefer, *Nature Materials* **6**, 853 (2007).
[24] R. Janes and e. Moore, *Metal-Ligand Bonding*, The Open University, Cambridge, UK, 2004.
[25] J. L. Jambor, J. e. Dutrizac, A. C. Roberts, J. D. Grice, and J. T. Szymański,

Canadian Mineralogist **34**, 61 (1996).
[26] J. D. Grice, J. T. Szymański, and J. L. Jambor, *Canadian Mineralogist* **34**, 73 (1996)
[27] B. M. Bartlett, *Synthesis, Structure, and Magnetic Properties of Extended 2-D Triangular Lattices,* PhD thesis, Massachusetts Institute of Technology, 2005.
[28] Private Communication with Dr. Shaoyan Chu.
[29] W. Krause, H.-J. Bernhardt, R. S. W. Braithwaite, U. Kolitsch and R. Pritchard, *Mineral Magazine* **70**, 329-340 (2006).
[30] E. A. Nytko, *Synthesis, Structure, and Magnetic Properties of Spin-1/2 Kagomé Antiferromagnetis*, PhD thesis, Massachusetts Institute of Technology, 2008.
[31] C. G. Shull and J. S. Smart, *Physical Review* **76**, 1256 (1949)
[32] Y. Ran, W.-H. Ko, P. A. Lee, and X.-G. Wen, *Physical Review Letters* **98**, 117205 (2007)
[33] C. Waldtmann, H.-U. Everts, B. Bernu, C. Lhuillier, P. Sindzingre, P. Lecheminant, and L. Pierre, *European Physical Journal B* **2**, 501 (1998).
[34] S. Ryu, O. I. Motrunich, J. Alicea, and M. P. A. Fisher, *Physical Review B* **75**, 184406 (2007).
[35] Y. Ran, M. Hermele, P. A. Lee, and X.-G. Wen, *Physical Review Letters* **98**, 117205 (2007).
[36] M. B. Hastings, *Physical Review B* **63**, 014413 (2001).
[37] M. Hermele, Y. Ran, P. A. Lee, and X.-G. Wen, *Physical Review B* **77**, 224413 (2008).
[38] N. Read and S. Sachdev, *Physical Review Letter* **66**, 1773 (1991).
[39] S. Sachdev, *Physical review B* **45**, 12377 (1992).
[40] F. Wang and A. Vishwanath, *Physical Review B* **74**, 174423 (2006).
[41] S. V. Isakov, T. Senthil, and Y. B. Kim, *Physical Review B* **72**, 174417 (2005).
[42] S.-S. Lee and P. A. Lee, Physical Review Letters 95, 036403 (2005).
[43] O. Motrunich, Physical Review B 72, 045105 (2005).
[44] M. E. Clissold, P. Leverett, P. A. Williams, D. E. Hibbs and E. H. Nickel, *Canadian Mineralogist* **45**, 317-320 (2007).
[45] D. M. Colchester, P. Leverett, M. E. Clissold, P. A. Williams, D. E. Hibbs, and E. H. Nickel, *Australian Journal of Mineralogy* **13**, 15-18 (2007).
[46] O. Ofer and A. Keren, *Physical Review B* **79**, 134424 (2009).
[47] Private Communication with Dr. Joel S. Helton.
[48] G. Misguich and C. Lhuillier, in *Frustrated Spin Systems*, edited by H. T. Diep (World Scientific, Singapore, 2004).
[49] C. Zeng and V. Elser, *Physics Review B* **42**, 8436 (1990).
[50] J. B. Marston and C. Zeng, *Journal of Applied Physics* **69**, 5962 (1991).
[51] R. R. P. Singh and D. A. Huse, *Physical Review Letter* **68**, 1766 (1992).
[52] S. Sachdev, *Physical Review B* **45**, 12377 (1992).
[53] C. Waldtmann, H.-U. Everts, B. Bernu, C. Lhuillier, P. Sindzingre, P. Lecheminant, and L. Pierre, *European Physical Journal B* **2**, 501 (1998).
[54] F. Wang and A. Vishwanath, *Physical Review B* **74**, 174423 (2006).
[55] T. Moriya, *Physical Review Letter* **4**, 228 (1960).
[56] T. Moriya, *Physical Review* **120**, 91 (1960).
[57] T. Moriya, "Weak Ferromagnetism", in *Magnetism Volume I*, edited by G. T. Rado and H. Suhl, Academic Press, New York, 1963.

[58] M. Tovar, K. S. Raman, and K. Shtengel, *Physical Review B* **79**, 024405 (2009).
[59] M. Rigol and R. R. P. Singh, *Physical Review B* **76**, 184403 (2007).
[60] M. Rigol and R. R. P. Singh, *Physical Review Letters* **98**, 207204 (2007).
[61] M. Elhajal, B. Canals, and C. Lacroix, *Physical Review B* **66**, 014422 (2002).

Appendix A. Crystallographic Data for HTH_1_11

Table A.1. Crystal data and structure refinement for HTH_1_1.

Identification code	08303	
Empirical formula	H6 Cl2 Cu3 O6 Zn	
Formula weight	428.94	
Temperature	100(2) K	
Wavelength	0.71073 Å	
Crystal system	Rhombohedral	
Space group	R-3m	
Unit cell dimensions	a = 6.8345(9) Å	α= 90°.
	b = 6.8345(9) Å	β= 90°.
	c = 14.0538(19) Å	γ = 120°.
Volume	568.51(13) $Å^3$	
Z	3	
Density (calculated)	3.759 Mg/m^3	
Absorption coefficient	12.113 mm^{-1}	
F(000)	615	
Crystal size	0.30 x 0.10 x 0.10 mm^3	
Theta range for data collection	3.74 to 29.50°.	
Index ranges	-9<=h<=9, -9<=k<=9, -19<=l<=19	
Reflections collected	3718	
Independent reflections	225 [R(int) = 0.0328]	
Completeness to theta = 29.50°	99.6 %	
Absorption correction	Semi-empirical from equivalents	
Max. and min. transmission	0.3772 and 0.1219	
Refinement method	Full-matrix least-squares on F^2	
Data / restraints / parameters	225 / 1 / 19	
Goodness-of-fit on F^2	1.264	
Final R indices [I>2sigma(I)]	R1 = 0.0135, wR2 = 0.0357	
R indices (all data)	R1 = 0.0138, wR2 = 0.0358	
Extinction coefficient	0.0063(5)	
Largest diff. peak and hole	0.452 and -0.403 $e.Å^{-3}$	

Table A.2. Atomic coordinates (x 10^4) and equivalent isotropic displacement parameters ($Å^2$x 10^3) for 08303. U(eq) is defined as one third of the trace of the orthogonalized U^{ij} tensor.

	x	y	z	U(eq)
Zn(1)	10000	0	5000	5(1)
Cu(2)	6667	-1667	3333	5(1)
Cl(3)	3333	-3333	4714(1)	8(1)
O(1)	8725(1)	1275(1)	3948(1)	8(1)

Table A.3. Bond lengths [Å] and angles [°] for 08303.

Zn(1)-O(1)	2.1132(16)
Zn(1)-O(1)#1	2.1132(16)
Zn(1)-O(1)#2	2.1132(16)
Zn(1)-O(1)#3	2.1132(16)
Zn(1)-O(1)#4	2.1132(16)
Zn(1)-O(1)#5	2.1132(16)
Zn(1)-Cu(2)#2	3.0625(3)
Zn(1)-Cu(2)#5	3.0625(3)
Zn(1)-Cu(2)	3.0625(3)
Zn(1)-Cu(2)#6	3.0625(3)
Zn(1)-Cu(2)#7	3.0625(3)
Zn(1)-Cu(2)#8	3.0626(3)
Cu(2)-O(1)#9	1.9843(8)
Cu(2)-O(1)#2	1.9843(8)
Cu(2)-O(1)	1.9843(8)
Cu(2)-O(1)#10	1.9843(8)
Cu(2)-Cl(3)	2.7678(6)
Cu(2)-Cl(3)#10	2.7678(6)
Cu(2)-Zn(1)#11	3.0625(3)
Cl(3)-Cu(2)#12	2.7677(6)
Cl(3)-Cu(2)#13	2.7678(6)
O(1)-Cu(2)#5	1.9843(8)
O(1)-H(1)	0.831(18)
O(1)-Zn(1)-O(1)#1	103.59(6)
O(1)-Zn(1)-O(1)#2	76.41(6)
O(1)#1-Zn(1)-O(1)#2	180.0
O(1)-Zn(1)-O(1)#3	180.0
O(1)#1-Zn(1)-O(1)#3	76.41(6)
O(1)#2-Zn(1)-O(1)#3	103.59(6)
O(1)-Zn(1)-O(1)#4	103.59(6)
O(1)#1-Zn(1)-O(1)#4	76.41(6)
O(1)#2-Zn(1)-O(1)#4	103.59(6)
O(1)#3-Zn(1)-O(1)#4	76.41(6)

O(1)-Zn(1)-O(1)#5	76.41(6)
O(1)#1-Zn(1)-O(1)#5	103.59(6)
O(1)#2-Zn(1)-O(1)#5	76.41(6)
O(1)#3-Zn(1)-O(1)#5	103.59(6)
O(1)#4-Zn(1)-O(1)#5	180.0
O(1)-Zn(1)-Cu(2)#2	85.68(4)
O(1)#1-Zn(1)-Cu(2)#2	139.94(2)
O(1)#2-Zn(1)-Cu(2)#2	40.06(2)
O(1)#3-Zn(1)-Cu(2)#2	94.32(4)
O(1)#4-Zn(1)-Cu(2)#2	139.94(2)
O(1)#5-Zn(1)-Cu(2)#2	40.06(2)
O(1)-Zn(1)-Cu(2)#5	40.06(2)
O(1)#1-Zn(1)-Cu(2)#5	94.32(4)
O(1)#2-Zn(1)-Cu(2)#5	85.68(4)
O(1)#3-Zn(1)-Cu(2)#5	139.94(2)
O(1)#4-Zn(1)-Cu(2)#5	139.94(2)
O(1)#5-Zn(1)-Cu(2)#5	40.06(2)
Cu(2)#2-Zn(1)-Cu(2)#5	67.825(8)
O(1)-Zn(1)-Cu(2)	40.06(2)
O(1)#1-Zn(1)-Cu(2)	139.94(2)
O(1)#2-Zn(1)-Cu(2)	40.06(2)
O(1)#3-Zn(1)-Cu(2)	139.94(2)
O(1)#4-Zn(1)-Cu(2)	94.32(4)
O(1)#5-Zn(1)-Cu(2)	85.68(4)
Cu(2)#2-Zn(1)-Cu(2)	67.824(8)
Cu(2)#5-Zn(1)-Cu(2)	67.824(9)
O(1)-Zn(1)-Cu(2)#6	139.94(2)
O(1)#1-Zn(1)-Cu(2)#6	40.05(2)
O(1)#2-Zn(1)-Cu(2)#6	139.95(2)
O(1)#3-Zn(1)-Cu(2)#6	40.06(2)
O(1)#4-Zn(1)-Cu(2)#6	85.68(4)
O(1)#5-Zn(1)-Cu(2)#6	94.32(4)
Cu(2)#2-Zn(1)-Cu(2)#6	112.178(8)
Cu(2)#5-Zn(1)-Cu(2)#6	112.176(8)
Cu(2)-Zn(1)-Cu(2)#6	180.0
O(1)-Zn(1)-Cu(2)#7	139.94(2)

O(1)#1-Zn(1)-Cu(2)#7	85.68(4)
O(1)#2-Zn(1)-Cu(2)#7	94.32(4)
O(1)#3-Zn(1)-Cu(2)#7	40.06(2)
O(1)#4-Zn(1)-Cu(2)#7	40.05(2)
O(1)#5-Zn(1)-Cu(2)#7	139.95(2)
Cu(2)#2-Zn(1)-Cu(2)#7	112.178(8)
Cu(2)#5-Zn(1)-Cu(2)#7	180.0
Cu(2)-Zn(1)-Cu(2)#7	112.177(8)
Cu(2)#6-Zn(1)-Cu(2)#7	67.823(8)
O(1)-Zn(1)-Cu(2)#8	94.32(4)
O(1)#1-Zn(1)-Cu(2)#8	40.06(2)
O(1)#2-Zn(1)-Cu(2)#8	139.94(2)
O(1)#3-Zn(1)-Cu(2)#8	85.68(4)
O(1)#4-Zn(1)-Cu(2)#8	40.06(2)
O(1)#5-Zn(1)-Cu(2)#8	139.94(2)
Cu(2)#2-Zn(1)-Cu(2)#8	180.0
Cu(2)#5-Zn(1)-Cu(2)#8	112.175(8)
Cu(2)-Zn(1)-Cu(2)#8	112.176(8)
Cu(2)#6-Zn(1)-Cu(2)#8	67.822(8)
Cu(2)#7-Zn(1)-Cu(2)#8	67.822(9)
O(1)#9-Cu(2)-O(1)#2	180.0
O(1)#9-Cu(2)-O(1)	97.61(9)
O(1)#2-Cu(2)-O(1)	82.39(9)
O(1)#9-Cu(2)-O(1)#10	82.39(9)
O(1)#2-Cu(2)-O(1)#10	97.61(9)
O(1)-Cu(2)-O(1)#10	180.0
O(1)#9-Cu(2)-Cl(3)	82.38(4)
O(1)#2-Cu(2)-Cl(3)	97.62(4)
O(1)-Cu(2)-Cl(3)	97.62(4)
O(1)#10-Cu(2)-Cl(3)	82.38(4)
O(1)#9-Cu(2)-Cl(3)#10	97.62(4)
O(1)#2-Cu(2)-Cl(3)#10	82.38(4)
O(1)-Cu(2)-Cl(3)#10	82.38(4)
O(1)#10-Cu(2)-Cl(3)#10	97.62(4)
Cl(3)-Cu(2)-Cl(3)#10	180.0
O(1)#9-Cu(2)-Zn(1)	136.74(5)

O(1)#2-Cu(2)-Zn(1)	43.26(5)
O(1)-Cu(2)-Zn(1)	43.26(5)
O(1)#10-Cu(2)-Zn(1)	136.74(5)
Cl(3)-Cu(2)-Zn(1)	85.574(16)
Cl(3)#10-Cu(2)-Zn(1)	94.428(16)
O(1)#9-Cu(2)-Zn(1)#11	43.26(5)
O(1)#2-Cu(2)-Zn(1)#11	136.74(5)
O(1)-Cu(2)-Zn(1)#11	136.74(5)
O(1)#10-Cu(2)-Zn(1)#11	43.26(5)
Cl(3)-Cu(2)-Zn(1)#11	94.427(16)
Cl(3)#10-Cu(2)-Zn(1)#11	85.572(16)
Zn(1)-Cu(2)-Zn(1)#11	180.0
Cu(2)#12-Cl(3)-Cu(2)#13	76.24(2)
Cu(2)#12-Cl(3)-Cu(2)	76.24(2)
Cu(2)#13-Cl(3)-Cu(2)	76.24(2)
Cu(2)#5-O(1)-Cu(2)	118.87(7)
Cu(2)#5-O(1)-Zn(1)	96.68(5)
Cu(2)-O(1)-Zn(1)	96.68(5)
Cu(2)#5-O(1)-H(1)	114.1(6)
Cu(2)-O(1)-H(1)	114.1(6)
Zn(1)-O(1)-H(1)	113.5(19)

Symmetry transformations used to generate equivalent atoms:

#1 y+1,-x+y+1,-z+1 #2 -y+1,x-y-1,z #3 -x+2,-y,-z+1

#4 x-y,x-1,-z+1 #5 -x+y+2,-x+1,z #6 x+2/3,y+1/3,z+1/3

#7 -x+y+5/3,-x+1/3,z+1/3 #8 -y+2/3,x-y-2/3,z+1/3

#9 y+1/3,-x+y+2/3,-z+2/3 #10 -x+4/3,-y-1/3,-z+2/3

#11 x-2/3,y-1/3,z-1/3 #12 -x+y+1,-x,z #13 -y,x-y-1,z

Table A.4. Anisotropic displacement parameters ($Å^2 x\ 10^3$) for 08303. The anisotropic displacement factor exponent takes the form: $-2\pi^2[\ h^2\ a^{*2}U^{11} + ...\ + 2\ h\ k\ a^*\ b^*\ U^{12}\ ]$

	U^{11}	U^{22}	U^{33}	U^{23}	U^{13}	U^{12}
Zn(1)	6(1)	6(1)	5(1)	0	0	3(1)
Cu(2)	5(1)	4(1)	6(1)	-1(1)	-1(1)	2(1)
Cl(3)	8(1)	8(1)	7(1)	0	0	4(1)
O(1)	8(1)	8(1)	10(1)	-1(1)	1(1)	4(1)

Table A.5. Hydrogen coordinates (x 10^4) and isotropic displacement parameters ($Å^2$x 10^3) for 08303.

	x	y	z	U(eq)
H(1)	8074(17)	1926(17)	4170(18)	10

Table A.6. Hydrogen bonds for 08303 [Å and °].

D-H...A	d(D-H)	d(H...A)	d(D...A)	<(DHA)
O(1)-H(1)...Cl(3)	0.831(18)	3.515(7)	3.6131(7)	90.1(6)

Symmetry transformations used to generate equivalent atoms:

#1 y+1,-x+y+1,-z+1 #2 -y+1,x-y-1,z #3 -x+2,-y,-z+1

#4 x-y,x-1,-z+1 #5 -x+y+2,-x+1,z #6 x+2/3,y+1/3,z+1/3

#7 -x+y+5/3,-x+1/3,z+1/3 #8 -y+2/3,x-y-2/3,z+1/3

#9 y+1/3,-x+y+2/3,-z+2/3 #10 -x+4/3,-y-1/3,-z+2/3

#11 x-2/3,y-1/3,z-1/3 #12 -x+y+1,-x,z #13 -y,x-y-1,z

Appendix B. Crystallographic Data for HTH_4_45

Table B.1. Crystal data and structure refinement for HTH_4_41.

Identification code	09211_2	
Empirical formula	H6 Cl2 Cu3 O6 Zn	
Formula weight	428.94	
Temperature	100(2) K	
Wavelength	0.71073 Å	
Crystal system	Rhombohedral	
Space group	R-3m	
Unit cell dimensions	a = 6.8300(12) Å	α= 90°.
	b = 6.8300(12) Å	β= 90°.
	c = 14.049(3) Å	γ = 120°.
Volume	567.57(17) $Å^3$	
Z	3	
Density (calculated)	3.765 Mg/m^3	
Absorption coefficient	12.133 mm^{-1}	
F(000)	615	
Crystal size	0.35 x 0.10 x 0.05 mm^3	
Theta range for data collection	3.74 to 30.52°.	
Index ranges	-9<=h<=8, -9<=k<=9, -19<=l<=19	
Reflections collected	2847	
Independent reflections	240 [R(int) = 0.0409]	
Completeness to theta = 30.52°	98.8 %	
Absorption correction	Semi-empirical from equivalents	
Max. and min. transmission	0.5822 and 0.1006	
Refinement method	Full-matrix least-squares on F^2	
Data / restraints / parameters	240 / 0 / 19	
Goodness-of-fit on F^2	1.220	
Final R indices [I>2sigma(I)]	R1 = 0.0183, wR2 = 0.0420	
R indices (all data)	R1 = 0.0187, wR2 = 0.0422	
Extinction coefficient	0.0065(5)	
Largest diff. peak and hole	0.940 and -0.631 $e.Å^{-3}$	

Table B.2. Atomic coordinates (x 10^4) and equivalent isotropic displacement parameters ($Å^2$x 10^3) for 09211_2. U(eq) is defined as one third of the trace of the orthogonalized U^{ij} tensor.

	x	y	z	U(eq)
Zn(1)	10000	0	5000	5(1)
Cu(2)	6667	-1667	3333	5(1)
Cl(3)	3333	-3333	4714(1)	8(1)
O(1)	8726(2)	1274(2)	3947(1)	8(1)

Table B.3. Bond lengths [Å] and angles [°] for 09211_2.

Zn(1)-O(1)#1	2.1121(19)
Zn(1)-O(1)#2	2.1121(19)
Zn(1)-O(1)	2.1121(19)
Zn(1)-O(1)#3	2.1121(19)
Zn(1)-O(1)#4	2.1121(19)
Zn(1)-O(1)#5	2.1121(19)
Zn(1)-Cu(2)#2	3.0610(4)
Zn(1)-Cu(2)#5	3.0610(4)
Zn(1)-Cu(2)	3.0611(4)
Zn(1)-Cu(2)#6	3.0611(4)
Zn(1)-Cu(2)#7	3.0611(4)
Zn(1)-Cu(2)#8	3.0612(4)
Cu(2)-O(1)#9	1.9826(9)
Cu(2)-O(1)#2	1.9827(9)
Cu(2)-O(1)	1.9827(9)
Cu(2)-O(1)#10	1.9827(9)
Cu(2)-Cl(3)	2.7660(8)
Cu(2)-Cl(3)#10	2.7660(8)
Cu(2)-Zn(1)#11	3.0611(4)
Cl(3)-Cu(2)#12	2.7659(8)
Cl(3)-Cu(2)#13	2.7660(8)
O(1)-Cu(2)#5	1.9826(9)
O(1)-H(1)	0.75(4)
O(1)#1-Zn(1)-O(1)#2	180.0
O(1)#1-Zn(1)-O(1)	103.65(8)
O(1)#2-Zn(1)-O(1)	76.35(8)
O(1)#1-Zn(1)-O(1)#3	76.35(8)
O(1)#2-Zn(1)-O(1)#3	103.65(8)
O(1)-Zn(1)-O(1)#3	180.00(7)
O(1)#1-Zn(1)-O(1)#4	76.35(8)
O(1)#2-Zn(1)-O(1)#4	103.65(8)
O(1)-Zn(1)-O(1)#4	103.65(8)
O(1)#3-Zn(1)-O(1)#4	76.35(8)

O(1)#1-Zn(1)-O(1)#5	103.65(8)
O(1)#2-Zn(1)-O(1)#5	76.35(8)
O(1)-Zn(1)-O(1)#5	76.35(8)
O(1)#3-Zn(1)-O(1)#5	103.65(8)
O(1)#4-Zn(1)-O(1)#5	180.0
O(1)#1-Zn(1)-Cu(2)#2	139.96(3)
O(1)#2-Zn(1)-Cu(2)#2	40.04(3)
O(1)-Zn(1)-Cu(2)#2	85.64(5)
O(1)#3-Zn(1)-Cu(2)#2	94.36(5)
O(1)#4-Zn(1)-Cu(2)#2	139.96(3)
O(1)#5-Zn(1)-Cu(2)#2	40.04(3)
O(1)#1-Zn(1)-Cu(2)#5	94.36(5)
O(1)#2-Zn(1)-Cu(2)#5	85.64(5)
O(1)-Zn(1)-Cu(2)#5	40.04(3)
O(1)#3-Zn(1)-Cu(2)#5	139.96(3)
O(1)#4-Zn(1)-Cu(2)#5	139.96(3)
O(1)#5-Zn(1)-Cu(2)#5	40.04(3)
Cu(2)#2-Zn(1)-Cu(2)#5	67.810(11)
O(1)#1-Zn(1)-Cu(2)	139.96(3)
O(1)#2-Zn(1)-Cu(2)	40.04(3)
O(1)-Zn(1)-Cu(2)	40.04(3)
O(1)#3-Zn(1)-Cu(2)	139.96(3)
O(1)#4-Zn(1)-Cu(2)	94.36(5)
O(1)#5-Zn(1)-Cu(2)	85.64(5)
Cu(2)#2-Zn(1)-Cu(2)	67.809(11)
Cu(2)#5-Zn(1)-Cu(2)	67.810(11)
O(1)#1-Zn(1)-Cu(2)#6	40.03(3)
O(1)#2-Zn(1)-Cu(2)#6	139.97(3)
O(1)-Zn(1)-Cu(2)#6	139.96(3)
O(1)#3-Zn(1)-Cu(2)#6	40.04(3)
O(1)#4-Zn(1)-Cu(2)#6	85.64(5)
O(1)#5-Zn(1)-Cu(2)#6	94.36(5)
Cu(2)#2-Zn(1)-Cu(2)#6	112.192(11)
Cu(2)#5-Zn(1)-Cu(2)#6	112.191(11)
Cu(2)-Zn(1)-Cu(2)#6	180.0
O(1)#1-Zn(1)-Cu(2)#7	85.64(5)

O(1)#2-Zn(1)-Cu(2)#7	94.36(5)
O(1)-Zn(1)-Cu(2)#7	139.96(3)
O(1)#3-Zn(1)-Cu(2)#7	40.04(3)
O(1)#4-Zn(1)-Cu(2)#7	40.03(3)
O(1)#5-Zn(1)-Cu(2)#7	139.97(3)
Cu(2)#2-Zn(1)-Cu(2)#7	112.192(11)
Cu(2)#5-Zn(1)-Cu(2)#7	180.0
Cu(2)-Zn(1)-Cu(2)#7	112.191(11)
Cu(2)#6-Zn(1)-Cu(2)#7	67.808(11)
O(1)#1-Zn(1)-Cu(2)#8	40.04(3)
O(1)#2-Zn(1)-Cu(2)#8	139.96(3)
O(1)-Zn(1)-Cu(2)#8	94.36(5)
O(1)#3-Zn(1)-Cu(2)#8	85.64(5)
O(1)#4-Zn(1)-Cu(2)#8	40.04(3)
O(1)#5-Zn(1)-Cu(2)#8	139.96(3)
Cu(2)#2-Zn(1)-Cu(2)#8	180.0
Cu(2)#5-Zn(1)-Cu(2)#8	112.190(11)
Cu(2)-Zn(1)-Cu(2)#8	112.191(11)
Cu(2)#6-Zn(1)-Cu(2)#8	67.808(11)
Cu(2)#7-Zn(1)-Cu(2)#8	67.808(11)
O(1)#9-Cu(2)-O(1)#2	180.0
O(1)#9-Cu(2)-O(1)	97.64(11)
O(1)#2-Cu(2)-O(1)	82.36(11)
O(1)#9-Cu(2)-O(1)#10	82.36(11)
O(1)#2-Cu(2)-O(1)#10	97.64(11)
O(1)-Cu(2)-O(1)#10	180.0
O(1)#9-Cu(2)-Cl(3)	82.36(5)
O(1)#2-Cu(2)-Cl(3)	97.64(5)
O(1)-Cu(2)-Cl(3)	97.64(5)
O(1)#10-Cu(2)-Cl(3)	82.36(5)
O(1)#9-Cu(2)-Cl(3)#10	97.64(5)
O(1)#2-Cu(2)-Cl(3)#10	82.36(5)
O(1)-Cu(2)-Cl(3)#10	82.36(5)
O(1)#10-Cu(2)-Cl(3)#10	97.64(5)
Cl(3)-Cu(2)-Cl(3)#10	180.0
O(1)#9-Cu(2)-Zn(1)	136.74(5)

O(1)#2-Cu(2)-Zn(1)	43.26(5)
O(1)-Cu(2)-Zn(1)	43.26(5)
O(1)#10-Cu(2)-Zn(1)	136.74(5)
Cl(3)-Cu(2)-Zn(1)	85.56(2)
Cl(3)#10-Cu(2)-Zn(1)	94.44(2)
O(1)#9-Cu(2)-Zn(1)#11	43.26(5)
O(1)#2-Cu(2)-Zn(1)#11	136.74(5)
O(1)-Cu(2)-Zn(1)#11	136.74(5)
O(1)#10-Cu(2)-Zn(1)#11	43.26(5)
Cl(3)-Cu(2)-Zn(1)#11	94.44(2)
Cl(3)#10-Cu(2)-Zn(1)#11	85.56(2)
Zn(1)-Cu(2)-Zn(1)#11	180.0
Cu(2)#12-Cl(3)-Cu(2)#13	76.24(2)
Cu(2)#12-Cl(3)-Cu(2)	76.24(2)
Cu(2)#13-Cl(3)-Cu(2)	76.24(2)
Cu(2)#5-O(1)-Cu(2)	118.91(9)
Cu(2)#5-O(1)-Zn(1)	96.71(6)
Cu(2)-O(1)-Zn(1)	96.71(6)
Cu(2)#5-O(1)-H(1)	114.8(8)
Cu(2)-O(1)-H(1)	114.8(8)
Zn(1)-O(1)-H(1)	111(3)

Symmetry transformations used to generate equivalent atoms:

#1 y+1,-x+y+1,-z+1 #2 -y+1,x-y-1,z #3 -x+2,-y,-z+1

#4 x-y,x-1,-z+1 #5 -x+y+2,-x+1,z #6 x+2/3,y+1/3,z+1/3

#7 -x+y+5/3,-x+1/3,z+1/3 #8 -y+2/3,x-y-2/3,z+1/3

#9 y+1/3,-x+y+2/3,-z+2/3 #10 -x+4/3,-y-1/3,-z+2/3

#11 x-2/3,y-1/3,z-1/3 #12 -x+y+1,-x,z #13 -y,x-y-1,z

Table B.4. Anisotropic displacement parameters ($Å^2 x\ 10^3$) for 09211_2. The anisotropic displacement factor exponent takes the form: $-2\pi^2[\ h^2\ a^{*2}U^{11} + ... + 2\ h\ k\ a^*\ b^*\ U^{12}\ ]$

	U^{11}	U^{22}	U^{33}	U^{23}	U^{13}	U^{12}
Zn(1)	5(1)	5(1)	5(1)	0	0	3(1)
Cu(2)	4(1)	4(1)	6(1)	-1(1)	-1(1)	2(1)
Cl(3)	8(1)	8(1)	7(1)	0	0	4(1)
O(1)	7(1)	7(1)	9(1)	0(1)	0(1)	4(1)

Table B.5. Hydrogen coordinates (x 10^4) and isotropic displacement parameters ($Å^2$x 10^3) for 09211_2.

	x	y	z	U(eq)
H(1)	8150(40)	1850(40)	4170(20)	9